

THESIS

DESIGN OF CONTROL TOOLS FOR USE IN MICROGRID SIMULATIONS

Submitted by

Avpreet Singh Othee

Department of Electrical and Computer Engineering

In partial fulfillment of the requirements

For the Degree of Master of Science

Colorado State University

Fort Collins, Colorado

Summer 2018

Master's Committee:

Advisor: Peter M. Young

Daniel Zimmerle

George Collins

Copyright by Avpreet Singh Othee 2018

All Rights Reserved

ABSTRACT

DESIGN OF CONTROL TOOLS FOR USE IN MICROGRID SIMULATIONS

New technologies are transforming the way electricity is delivered and consumed. In the past two decades, a large amount of research has been done on smart grids and microgrids. This can be attributed to two factors. First is the proliferation of internet. Internet today is as ubiquitous as electricity. This has spawned a new area of technology called the internet of things (IoT). It gives us the ability to connect almost any device to the internet and harness the data. IoT finds use in smart grids that allow utility companies to deliver electricity efficiently. The other factor is the advancement in renewable sources of electricity and high power semiconductors coupled with their decreasing cost. These new sources disrupt the traditional way of electricity production and delivery, putting an increased focus on distributed power generation and microgrids.

A microgrid is different from a utility grid. The difference is in the size of the grid, power level, a variety of possible sources and the way these are tied together. These characteristics lead to some unique control challenges. Today's appliances and consumer goods are powered using a standardized AC power. Thus a microgrid must deliver uninterrupted and high quality power while at the same time taking into account the vastly different nature of the microsources that produce the power. This work describes control system tools for different power converters that will be used in simulating microgrids.

Simulations are important tool for any researcher. It allows researchers to test their research and theories at a greatly reduced cost. The process of design, testing and verification is an iterative process. Simulations allow a cost effective method of doing research, substituting the actual process of building experimental systems. This greatly reduces the amount of manpower and capital investment.

A microgrid consists of several building blocks. These building blocks can be categorized into microsources, energy stores, converters and the loads. Microsources are devices that produce elec-

tric power. For example, a photovoltaic panel is a microsource that produces DC power. Converters act as an interface between microsources and the grid. The constituent chapters in the document describe microsources and converters. The chapters describe the underlying control system and the simulation model of the system designed in Simulink.

Some of the tools described are derived from the MATLAB/Simulink Examples library. Original authors of the simulation models and systems have been duly credited. Colorado State University has a vibrant research community. The tools described in this thesis are geared to be used for research into microgrids. The tools are developed in a simulation software called Simulink. The tools would allow future researchers to rapidly build microgrid simulations and test new control system implementations etc.

The research described in the thesis builds upon the research by Han on natural gas engine based microgrid [1]. The control tools described here are used to construct a microgrid simulation. The microgrid is built around a natural gas engine. Due to the transport lag in delivering fuel, a natural gas engine exhibits significant deviation in the AC grid frequency when subjected to step load. The microgrid setup along with the control system described here, minimizes the frequency deviation, thus stabilizing the microgrid. Simulation results verify the working of the tools .

ACKNOWLEDGEMENTS

I would like to thank my advisor Dr. Peter Young for his guidance and valuable insights. This work would not have been possible without his feedback, constructive criticism and oversight. I enjoyed the occasional side talks about random topics that broadened my horizon and giving a personal touch to the job.

I would also like to thank members of my committee Dr. Daniel Zimmerle and Dr. George Collins for their oversight, comments and thoughtful questions.

I would like to thank Daniel Luckner for his support. I would especially like to thank Dr. Hamidreza Chitsaz for his support and letting me be a part of the CSU Robocup team. It has been a wonderful experience. It gave me an opportunity to interact with people from varied backgrounds and helped me explore the world of computer science.

Lastly I would like to thank my parents for their continued support and their unwavering faith in me. I would especially like to thank my sister for always being there to support me.

Avpreet Singh Othee

DEDICATION

To my parents.

Avtar and Preet

TABLE OF CONTENTS

| | | |
|-----------|--|----|
| | ABSTRACT | ii |
| | ACKNOWLEDGEMENTS | iv |
| | DEDICATION | v |
| | LIST OF TABLES | ix |
| | LIST OF FIGURES | x |
| Chapter 1 | Introduction | 1 |
| 1.1 | Simulink Simulation Setup | 2 |
| 1.2 | Document Structure | 5 |
| Chapter 2 | Microgrid Topologies | 6 |
| 2.1 | DC Bus Topology | 6 |
| 2.2 | AC Bus Topology | 8 |
| Chapter 3 | Generator | 10 |
| 3.1 | Engine | 10 |
| 3.1.1 | Engine Control | 13 |
| 3.2 | Synchronous Generator | 17 |
| 3.3 | AC grid frequency control as a power control technique | 20 |
| 3.4 | Multiple Generator Operation | 21 |
| 3.4.1 | Generator Synchronization | 25 |
| Chapter 4 | Photovoltaic Power System | 27 |
| 4.1 | Maximum Power Point Tracking | 29 |
| Chapter 5 | Battery Storage System | 36 |
| 5.1 | Battery Model | 37 |
| 5.2 | Battery Controller | 38 |

| | | |
|--------------|---|----|
| 5.2.1 | Lithium-ion Battery Charging Algorithm | 38 |
| 5.2.2 | Battery Controller Implementation in Simulink | 39 |
| Chapter 6 | Universal Bridge Converter | 43 |
| 6.1 | Reference frame theory and direct quadrature zero transformation | 43 |
| 6.2 | Three-phase Bridge Converter | 45 |
| 6.3 | Three-phase bridge converter as a PWM Rectifier | 47 |
| 6.3.1 | Unity power factor condition | 48 |
| 6.3.2 | Rectifier Control | 49 |
| 6.4 | Three-phase bridge converter as a grid forming inverter | 51 |
| 6.4.1 | Inverter Control | 52 |
| 6.5 | Three-phase bridge converter as a Grid Following / Grid Supporting Inverter | 53 |
| 6.5.1 | Inverter Control | 54 |
| Chapter 7 | Microgrid Simulation | 59 |
| 7.1 | Natural Gas Engine Based Microgrid with attached Storage System | 61 |
| 7.2 | Optimized settings for simulation | 67 |
| 7.2.1 | Power Electronics Devices modeling | 68 |
| 7.2.2 | Miscellaneous settings | 69 |
| Chapter 8 | Conclusion and Future Work | 70 |
| 8.1 | Future Work | 71 |
| 8.1.1 | Hardware-In-the-Loop Testing | 71 |
| 8.1.2 | Use of alternate storage technologies | 72 |
| 8.1.3 | Robust MIMO Control of the microgrid | 73 |
| Bibliography | | 75 |
| Appendix A | MPPT Algorithm | 81 |

| | | |
|------------|---|----|
| Appendix B | PID Algorithm | 82 |
| Appendix C | Additional tools and some implementations | 83 |
| Appendix D | Summary of important library components | 85 |

LIST OF TABLES

| | | |
|-----|---|----|
| 5.1 | Li-ion battery specifications. | 37 |
| 7.1 | Microgrid system specifications | 63 |

LIST OF FIGURES

| | | |
|-----|---|----|
| 1.1 | Simulink Simulation model Description | 4 |
| 2.1 | DC Bus Topology. | 7 |
| 2.2 | AC Bus Topology. | 9 |
| 3.1 | Natural gas engine Simulink model. | 11 |
| 3.2 | Natural gas engine Simulink model. | 13 |
| 3.3 | Natural gas engine control. | 15 |
| 3.4 | Natural gas engine response | 16 |
| 3.5 | Diesel engine response. | 17 |
| 3.6 | Synchronous generator circuit | 18 |
| 3.7 | Synchronous generator implementation in Simulink. | 20 |
| 3.8 | Fequency droop control | 23 |
| 4.1 | Equivalent circuit of a PV cell. | 27 |
| 4.2 | PV Voltage Current Curves. | 29 |
| 4.3 | Boost converter. | 31 |
| 4.4 | PV MPPT controller in Simulink | 32 |
| 4.5 | Power output with and without MPPT controller. | 34 |
| 4.6 | PV panel ouput power | 35 |
| 5.1 | Discharge curve for the battery. | 38 |
| 5.2 | Lithium-ion battery charging sequence. | 39 |
| 5.3 | Battery controller with converter. | 40 |
| 5.4 | Battery controller | 41 |
| 5.5 | Battery Controller GUI | 41 |
| 5.6 | Battery charging curve | 42 |

| | | |
|------|---|----|
| 6.1 | ABC to dq0 transformation. | 44 |
| 6.2 | Three-phase bridge converter. | 46 |
| 6.3 | Voltage and current axis in dq0 reference frame. | 49 |
| 6.4 | Rectifier Control. | 50 |
| 6.5 | Rectifier Outputs. | 51 |
| 6.6 | Grid Forming inverter control. | 52 |
| 6.7 | Grid forming inverter outputs. | 53 |
| 6.8 | Grid supporting inverter control | 54 |
| 6.9 | Grid supporting inverter Simulink implementationl | 56 |
| 6.10 | Grid supporting inverter controller GUI | 57 |
| 6.11 | Grid supporting inverter outputsl | 58 |
| 7.1 | Natural Gas Engine powered generator output. | 60 |
| 7.2 | Microgrid control with attached storage systeml | 61 |
| 7.3 | Simulink implementation of the microgrid | 64 |
| 7.4 | Microgrid control with attached storage systeml | 65 |
| 7.5 | Microgrid power share | 66 |
| 7.6 | Battery State of Charge | 67 |
| C.1 | Generator with accomapnying controllers | 83 |
| C.2 | Batterty controller example | 84 |

Chapter 1

Introduction

It is impossible to imagine modern human civilization without electricity. Utility grids have been the backbone of the energy infrastructure and have largely been unchanged since they were first introduced at the beginning of twentieth century. Utility grid due to its' centralized nature has some disadvantages. A recent example would be Hurricane Maria that hit the island of Puerto Rico in the fall of 2017. It knocked down most of the island's electricity grid, rendering almost all the island without power [2]. The issues associated with a centralized grid can be addressed by using distributed sources of energy and decentralizing the electricity grid. Recently, investment in renewable sources has gained a lot of momentum. Advancement in technologies that tap into these renewable sources have transformed the way electricity is consumed. Microgrids that utilize these renewable sources, combined with conventional sources have increasingly been used to mitigate the drawbacks associated with a conventional centralized utility grid. Microgrids installed in some locations in Puerto Rico continued to work even after the utility grid was down.

A microgrid is an enveloping term that refers to an electrical installation that might or might not be connected to the utility grid, but in itself has all the components of a grid. Microgrids are installed in remote areas that do not have access to the utility grid. Microgrids are also implemented in sensitive installations such as hospitals, airports etc. that require an uninterrupted power, even in the event of an outage in the utility grid. Microgrids may be installed in areas that have an abundance of one type of natural resource. A microgrid that can tap into such varied sources of energy leads to some interesting design challenges. This thesis is a small contribution towards solving those challenges.

This thesis describes the development of control systems in a commercial simulation software package. The control tools are aimed at design and simulation of power systems in microgrid. The text describes a simulation of a microgrid built around a natural gas engine. Potential application of such a microgrid would be in an off-site installation that has an easy access to natural gas.

It describes a proposed control system for this type of microgrid, and details construction of a simulation, utilizing the control tools described in the constituent chapters.

Various simulation software are available that can simulate electrical power systems and circuits. One such software is the MATLAB™ Simulink™ Simscape Power Systems, Specialized Technology. It is a set of specialized components and algorithms intended to be used in simulation of electrical power systems and power electronic devices [3]. The Specialized Technology components library is developed by Hydro-Québec. Using the library one can implement and simulate power systems. The Simulink environment can be used to implement control system that integrates with the power system components. Other simulation and data acquisition tools available in Simulink, coupled with MATLAB's toolboxes makes the Simulink a suitable choice for simulating control systems for electrical systems. The tools described here builds upon work done by Han and Dr. Peter Young at Colorado State University. Some tools are derived from the examples in "Simulink Simscape Sim Power Systems, Specialized Technology Toolbox".

1.1 Simulink Simulation Setup

A simulation is a replication of physical phenomenon or real world systems in a virtual setting. Physical systems are characterized by mathematical expressions (differential and algebraic equations) that are solved to get outputs, referred to as simulated outputs. In Simulink environment, these systems are arranged as visual blocks representing systems mimicking physical systems. Data flow between these systems is shown by interconnecting paths representing flow of data. The system is solved by a solver engine using numerical integration techniques. User can specify parameters for the engine such as, solver step time, solver type etc.

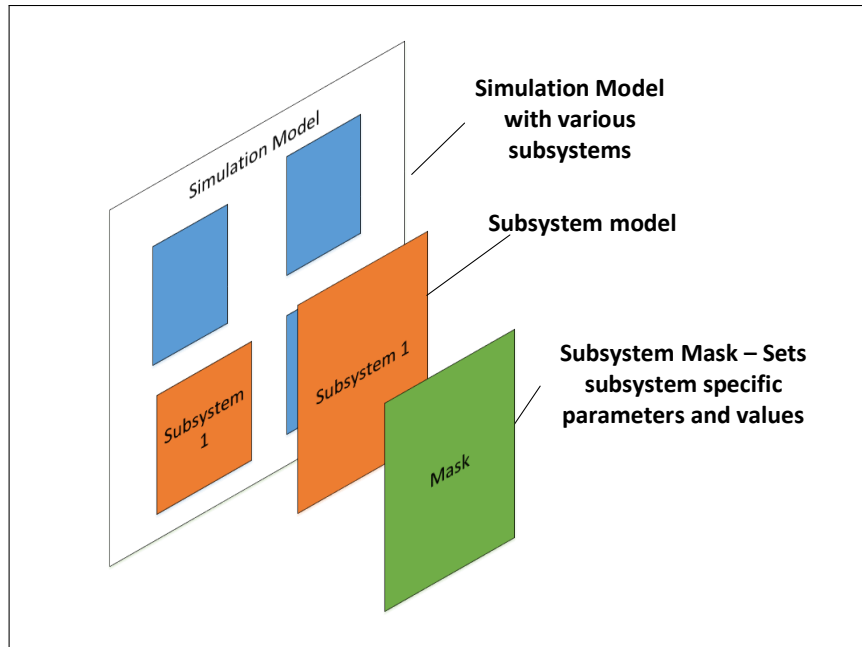
Simulation is stored in a model file. The model file stores all the information about the constituent subsystems and models in an XML format [4]. The building blocks of a Simulink simulation are Simulink blocks. A block is analogous to a function. Figure 1.1a shows a hierarchical visual breakdown of a simulation with various subsystems. The bottommost layer in the figure represents the simulation. The subsystem mask is a visual depiction of a subsystem. User inter-

acts with the mask when implementing the subsystem. The mask contains all the parameters and model specific values. These parameters give the user a high level of flexibility in customizing the subsystem to suit the simulation requirements. Figure 1.1b shows an actual subsystem mask along with the block parameters dialog box. The parameters can be assigned default values that can be changed later as desired.

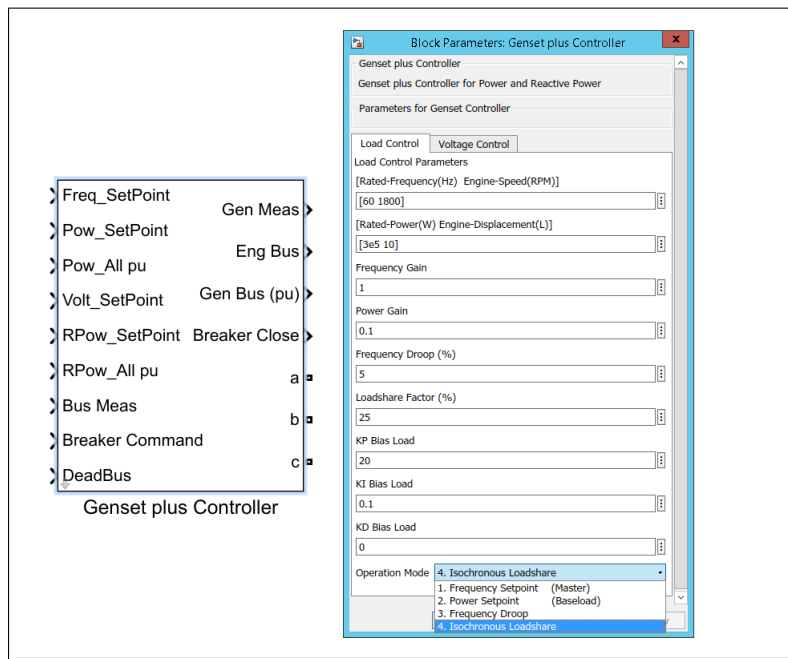
Simulink Sim Power Systems Specialized Technology Components Working

The Simulink Simscape Power Systems Specialized Technology Library is a simulation domain within Simulink . It lets a user simulate electrical components and power systems, otherwise simulated in specialized electrical simulation software. It combines two otherwise different simulation paradigms into one, adding a high level of flexibility towards system design and simulation. It is especially helpful from a controls point of view, for a controls designer working on control for power systems. A simulation using the Simscape Power Systems Specialized Technology components is distinguished from a regular Simulink system by a "Power GUI" block. The block sets various solver settings and options specific to the Specialized Technology library component. Besides solver settings, the block provides analysis tools that are useful for system analysis. A simulation using the Simscape Power Systems Specialized Technology components is executed in the following steps: [5]

1. The simulation is initialized and sorted into linear and nonlinear blocks.
2. The linear part of the simulation is converted into state-space equations. This linear part of the system is simulated using the S-Function blocks of the MATLAB. The nonlinear part is executed using predefined Simulink blocks.’
3. The simulation is built and stored inside the Powergui block. The electrical simulation and Simulink simulation reside in separate domains. Special interface blocks must be used to interchange data between these.



(a) Depiction of the layered architecture of a Simulink simulation model.



(b) Diesel Generator Controller mask showing various parameters

Figure 1.1: (a) Depiction of layered architecture. (b) A subsystem mask

1.2 Document Structure

This chapter provided some background information on the MATLAB/Simulink software. The rest of the thesis is structured as follows. Next chapter describes microgrid topologies, listing their potential usage, benefits and drawbacks. Chapter 3 describes a generator unit. It describes the modeling and control of an engine followed by description of a synchronous generator. This chapter then describes how multiple generators can be setup and controlled. Chapters 4 and 5 describe the photovoltaic system and the battery storage system. Chapter 6 describes control techniques for a three-phase bridge converter. Chapter 7 gives an example implementation of a microgrid using some of the tools developed and described in the thesis. The last chapter lists concluding remarks and suggestions for future work on further development of the library along with potential uses. It describes how simulation techniques such as HIL can be integrated with the tools developed here to further research into microgrids.

Chapter 2

Microgrid Topologies

Microgrid technologies are getting mainstream adoption due to many factors. One the factors driving this growth is the increasing affordability of renewable technologies such as wind and solar power. This has been supplemented by progress in material science that has increased the efficiency of these energy sources. Coupled with ever increasing demand for high capacity lithium-ion batteries and super-capacitors, microgrid engineers and designers have a myriad of electrical sources to choose from. All these factors when combined present a very promising picture for the microgrids. The abundance of energy sources pose a design and control challenge. These sources have different characteristics, response times and implementation constraints. A designer must be able to recognize these factors when designing a microgrid, to operate them at their full efficiency. The next two sections describe the two widely implemented microgrid topologies.

2.1 DC Bus Topology

In a microgrid installation, photovoltaic panel constitutes an important and noticeable component. This can be attributed to the availability of abundant sunlight and the decreasing cost of photovoltaic panels [6] [7]. Combined with storage units such as batteries and supercapacitors, the DC power constitute a large portion of modern day microgrids. Combining these factors with an ever-increasing shift towards DC load devices, it becomes inevitable to design a microgrid around the DC power. A significant amount of research and literature has used a DC bus based microgrid topologies [8] [9].

The thesis lays out a proposed microgrid topology constructed around a common DC bus. Figure 2.1 shows the schematic and the components of the proposed DC topology.

All the electrical sources are connected to a common DC bus. The sectioned blocks are power converters that interface with a source and the bus. The arrows underneath every converter block represents the power flow. The PV and the generators have unidirectional power converters that

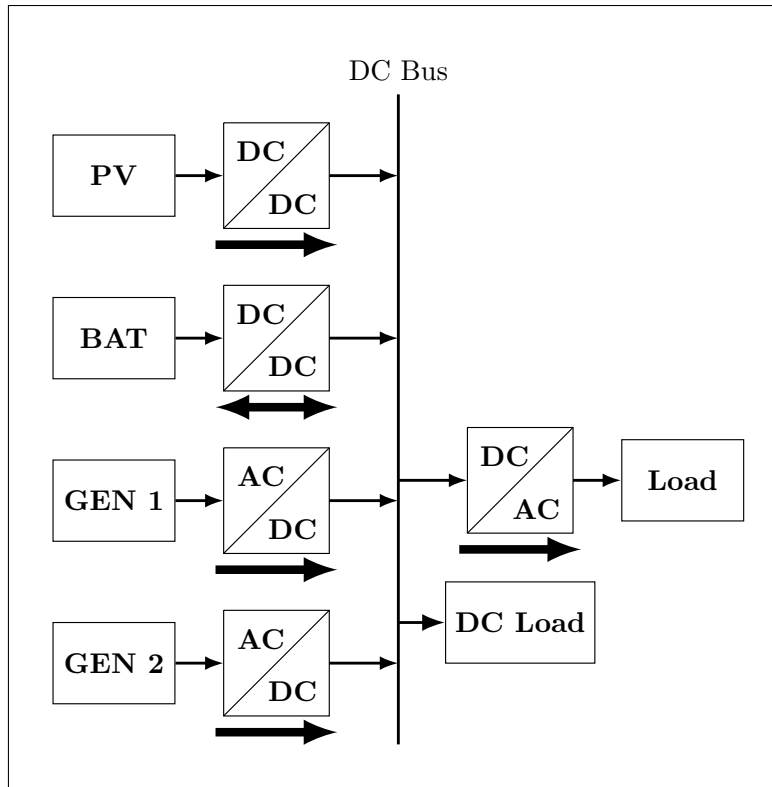


Figure 2.1: DC Bus Topology.

dump power into the DC bus. The battery is connected to the DC bus with a bi-directional DC to DC converter. This allows the battery to act as an energy buffer, supplying power to the DC bus when required. The bidirectional converter allows power flow into the battery during a charge cycle. A DC load can be directly connected to the bus.

Microgrids are designed to supplement or work with existing electrical infrastructure. Thus, an AC power converter is an essential component. The AC to DC converter (inverter), connected to a common DC bus, converts the DC power into AC power. All the AC loads are connected the AC bus driven by an inverter. The microgrids in this text are assumed to be working in islanded operation. Thus, the inverter has to generate the AC power without any external AC power prime mover. This type of inverter is called a grid forming inverter. Chapter 6 describes the simulation model and control of a grid forming inverter.

There are some advantages and disadvantages of using a DC bus based microgrid. Multiple generator units in an AC grid require grid synchronization to operate in parallel. Simultaneous

operation of these generators, acting as single power source require specialized controllers and infrastructure. These also require control strategies to control output power and maintain grid frequency. A DC bus based microgrid does not require these. The generator units have individual DC power converters (rectifiers), thus no grid synchronization is required.

The downside of this topology is the cost of converters and the added complexity associated with these. Each generator unit would require its own rectifier unit. The other disadvantage is the lack of a prime mover on the AC side. Inverters, as opposed to generators, do not have inertia associated with a rotor. The inertia can absorb mild fluctuations induced by load changes. This acts as to stabilize the grid against disturbances. In an inverter powered grid with virtually no inertia, an inductive load can induce unwanted harmonics and destabilize the grid frequency. Control systems have been designed that implement the concept of virtual inertia that can mitigate these issues [10].

2.2 AC Bus Topology

Another microgrid topology is where the DC and AC sources are separate. This topology is cost efficient as the microgrid can be setup by integrating new devices with existing electrical infrastructure, such as rural or remote grid installations. Figure 2.2 shows the schematic of an AC bus based microgrid topology. One can notice the difference the way the generators and the inverter are connected. The inverter is a bidirectional AC to DC converter. In a three-phase system, the AC to DC converter is a three phase bridge converter. The converter acts as a rectifier or inverter by selecting appropriate control algorithm and the desired flow of power. Chapter 6 describes three phase universal bridge and underlying rectifier or inverter control strategies. The bridge converter can push power into the DC bus to charge the battery when excess power is available on the AC side.

The inverter used in such configuration is a grid following or grid supporting inverter [11]. A grid supporting inverter converts DC power to AC power but is not the grid master. The inverter follows and maintains the AC power and frequency set by another AC source, usually a prime mover synchronous generator. When multiple generators are employed, the generators are syn-

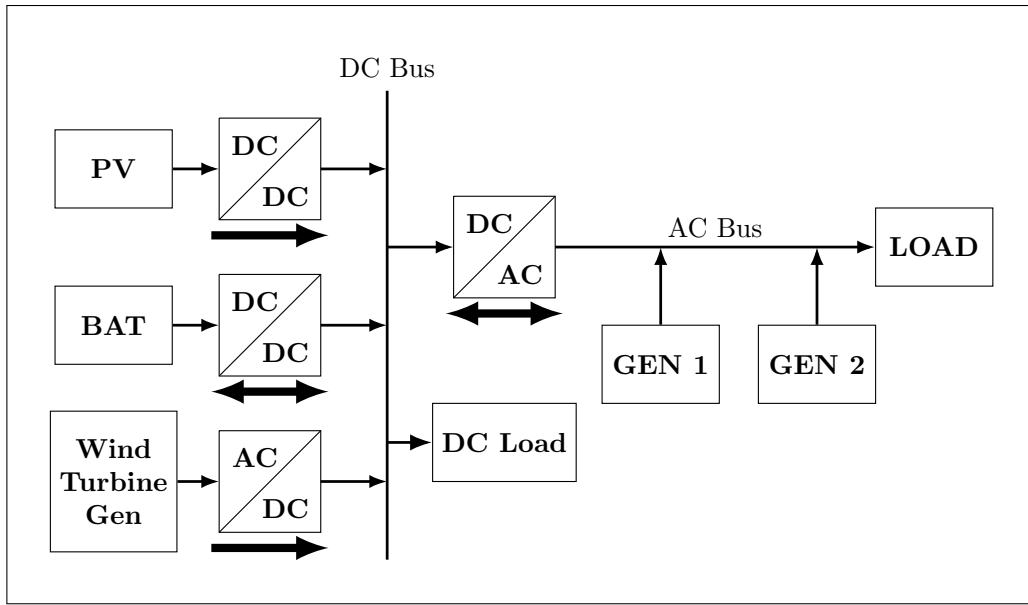


Figure 2.2: AC Bus Topology.

chronized to operate in phase producing power as a single power source. The synchronization and load sharing control strategies are discussed in the next chapter. Besides the above mentioned microgrid topologies, there are other possible configurations. Author aims to pursue research into these in the future.

Chapter 3

Generator

A generation unit is an essential component of a microgrid. Internal combustion engines have been around for over a century. Some of their characteristics make them indispensable for use in microgrids. Diesel engines can be modeled using simple linear models because of their predictable performance and quick transient response. The research in this text is geared towards designing of control systems for microgrids that are built using natural gas engines. This chapter describes the detailed Simulink model of a natural gas engine. The engine models used in this library were developed by Yi Han at Colorado State University [1]. The chapter then describes the working of synchronous generator and how multiple generators can be used in various configurations to achieve desired power output.

3.1 Engine

An engine is a complex machine with various mechanical systems working together. For a four stroke engine, the engine cycle can be summarized as follows. In the suction cycle, the piston draws fuel from the fuel inlet mechanism. Suction cycle is followed by the compression cycle, in which the piston moves upwards compressing the fuel-air mixture. Then follows the combustion cycle. It is also known as the power stroke. Power stroke is the one that counts for the actual power output from the engine. The combustion cycle is followed by the exhaust cycle. In this cycle the burnt gases from the previous cycle are expelled via the exhaust manifold. Engine consists of various subsystems that contribute to the engine cycle. Figure 3.1 shows the subsystems and their interconnections implemented as a Simulink simulation model. The subsystems and their working is described below.

The air filter is modeled as a giant orifice, thus, the air flow is calculated by standard compressible fluid flow equations [12]. Air filter subsystem composes the input section. It purifies the

air going into the combustion chamber. The air filter introduces a pressure drop and thus, is an essential modeling component.

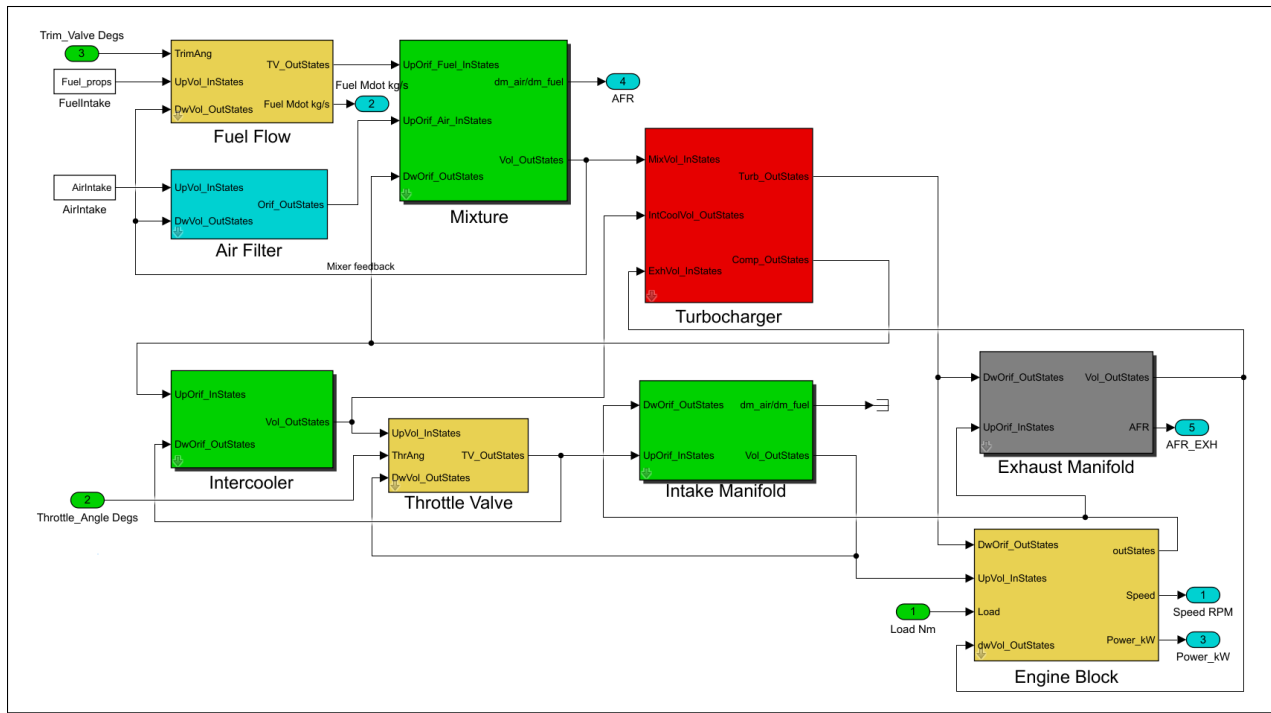


Figure 3.1: Natural gas engine Simulink model showing various subsystems.

The fuel valve controls the amount of fuel going into the engine. The amount of air and fuel mixture going into the engine is known as the Air to Fuel Ratio (AFR). The fuel value controls the AFR and is modeled as a butterfly valve. The mixer block models the mixing of the air and the fuel.

The mixer block output is then fed to the turbocharger. One can notice the output port ‘AFR’ is connected to the mixture block. The AFR output from the engine is used as control variable. A controlled AFR is necessary for increasing the engine efficiency [13]. In case of a natural gas engine, the AFR should be tightly controlled for the engine to operate [1].

The turbocharger consists of a turbine, compressor and a rotor. A turbocharger increases the inlet flow, thus, producing more power with the same size of engine displacement. The turbocharger subsystem models the subcomponents separately. It consists of a compressor that connects to a

turbine with a rotor. The compressor compresses the incoming fuel air mixture. The rotor acts as mechanical coupling between the compressor and the turbine. The outputs from the compressor and turbine are then fed into the inter-cooler and engine block, respectively.

The inter-cooler reduces the temperature of the compressed flow, thus, increasing the flow density, eventually generating more power. In the model, the inter-cooler is modeled as a volume element.

The throttle valve is modeled similarly to the inlet valve with some slight changes. It is the control element that controls the engine speed. Intake manifold distributes the air and fuel mixture into the cylinders for the combustion cycle. It is an important component of an engine due to the requirement of uniform distribution of the mixture to all cylinders. The manifold is modeled on the principle of conservation of energy and the ideal gas laws.

The engine block is the part of the model where actual combustion takes place, converting the heat energy into mechanical energy, hence generating the output torque. The mean indicated torque is the output torque of the engine. It is calculated by

$$T_i = m_f \cdot Q_{LHV} \cdot \eta_{ind} \quad (3.1)$$

where, m_f is the fuel mass in the cylinders, Q_{LHV} is the fuel lower heating value and η_{ind} is the indicated efficiency of the engine. The model computes the friction and pumping losses, thus presenting an accurate model of an actual engine.

Exhaust manifold collects the exhaust gases generated in the cylinders and vents them out. The exhaust manifold is modeled similarly as the intake manifold. In the model, one can notice the 'volume output states' from the exhaust manifold goes back into the intercooler. This is because some of the energy from the exhaust gases is extracted for increasing the inlet flow.

Figure 3.2 shows the Simulink subsystem mask for a natural gas engine. The library contains simulation models for diesel and natural gas engines. The models are highly detailed and customizable. This gives the controls designer a lot of flexibility in designing setting up the simulation for different engine models and sizes. Each subcomponent in the model can be adjusted from the top-

most mask. This flexibility to adjust or modify each subsystem allows the model to be accurate, thus, accurately modeling behavior of an actual engine. Usage and function of a subsystem mask was described in Chapter 1.

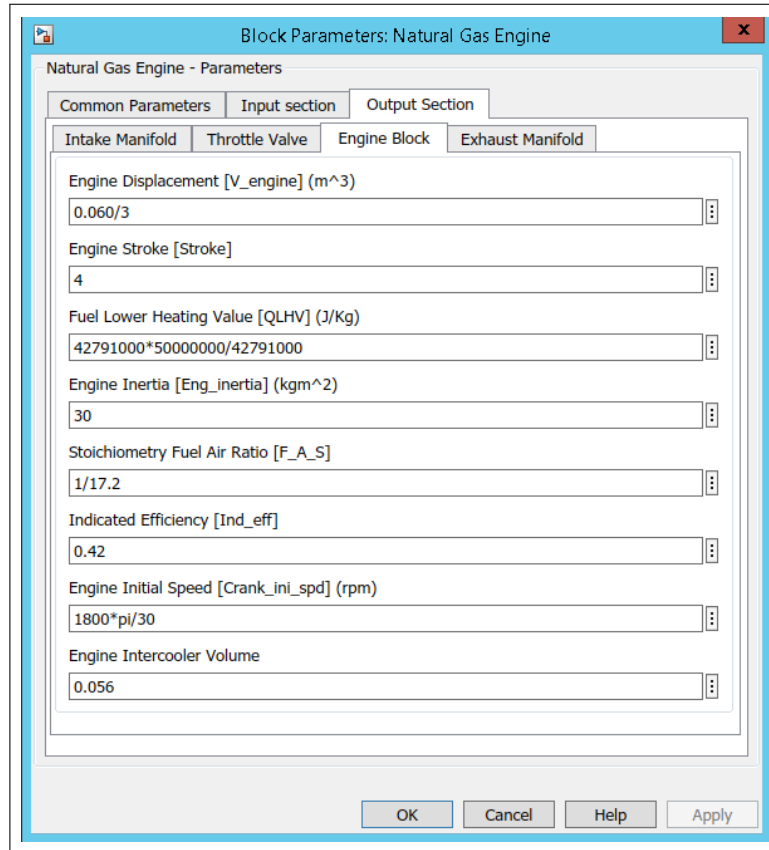


Figure 3.2: Natural gas engine Simulink model showing various subsystems.

3.1.1 Engine Control

Internal combustion engines like diesel and natural gas engines are widely used in small grid installations to drive a generator. Engines have a fundamental advantage over other forms of microsources such as wind and solar energy, such that the energy output is not dependent on environmental factors. AC grids operate at a fixed frequency that must be maintained for stable grid operation. For a synchronous generator, grid frequency is related to the engine RPM by

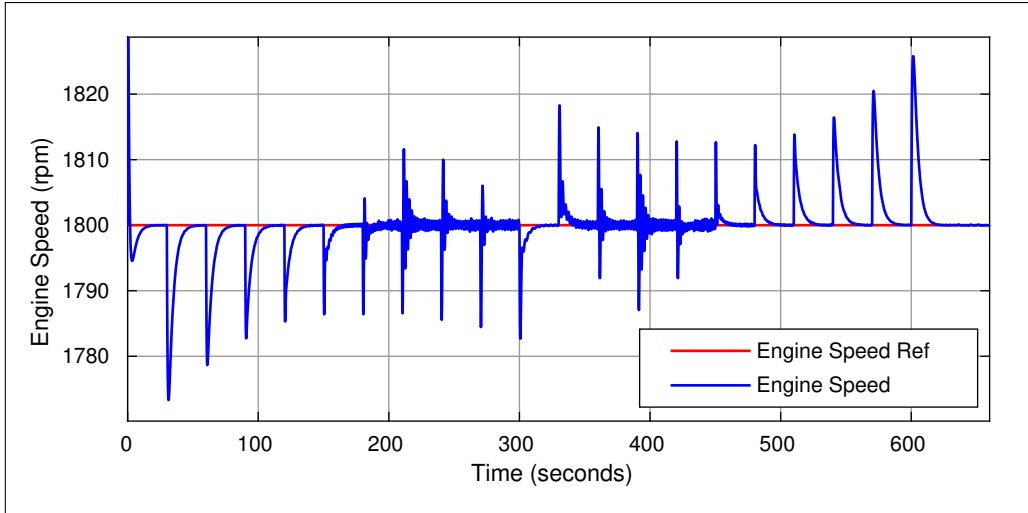
$$f = rpm \cdot \frac{P}{60} \quad (3.2)$$

where P is the number of pole pairs and rpm is the rotor rpm. Hence engine speed control is an essential component of microgrid control. Simple engine speed control in these simulation models is achieved using PID regulators, also called a governor. Chapter 8 discusses use of a MIMO controller for engine speed control. PID controller for engine speed controller is discussed below.

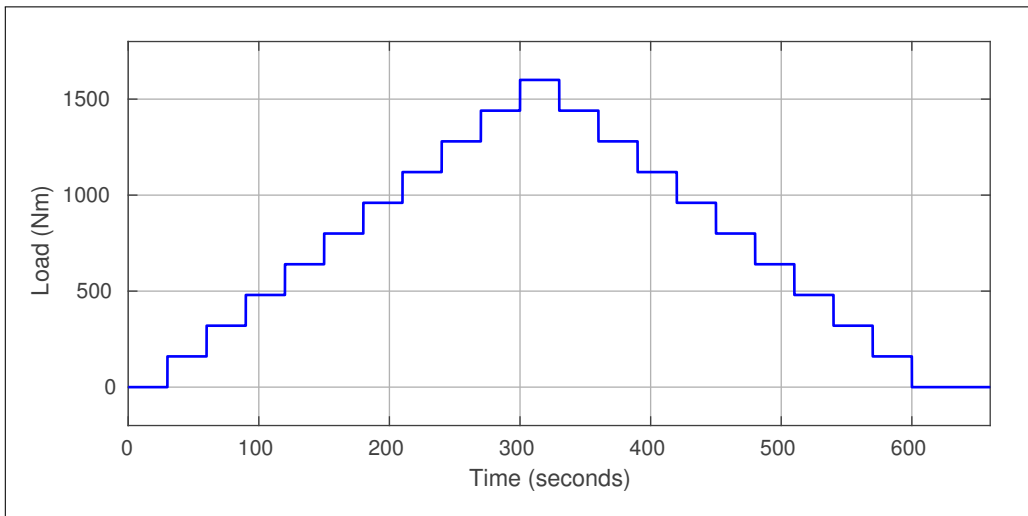
A change in the torque experienced by the engine affects the engine rpm. A PID controller measures the engine RPM and compares it with a set reference value. The error is fed to a PID regulator that generates a control output. The control output is the amount of fuel injected into the engine. Fuel control in an engine is achieved using a throttle valve, shown on the left as an input port connected to the throttle block in Figure 3.1. A PID controller is robust in the sense that one does not need to have detailed knowledge about underlying mathematical model of the plant. The PID gains are carefully tuned to achieve a reasonable performance. Simulation tools developed in the toolbox are intended towards microgrids built around a natural gas engine. In a natural gas engine, besides the control of engine output, another important control variable is the inlet Air to Fuel Ratio (AFR). For a lean burn natural gas engine, AFR should be tightly controlled.

Figure 3.3 shows the Simulink implementation of a natural gas engine. Notice there are two separate PID regulators for engine speed control and AFR control.

A natural gas engine is different from a diesel engine. In a diesel engine, the fuel is injected directly into the combustion chamber. In contrast, for a pre-mixed lean burn natural gas engine, fuel is injected before the turbocharger. This leads to a considerable fuel transport delay. Therefore a natural gas engine has a poor transient response to sudden load changes compared to a diesel engine. Figure 3.4b shows the engine speed output for a natural gas engine. The load on the engine is varied in steps, shown in Figure 3.4a. Engine speed reference is set at 1800 rpm. PID governor measures the error in the reference and the measured speed commanding a control output that injects fuel into the engine. Notice that after every step change in the load, the engine rpm shows a big variation. The PID regulator tries to maintain the reference. Engine speed settles to



(a) Engine Load.



(b) Natural gas engine speed response

Figure 3.4: Natural gas engine load input and speed response

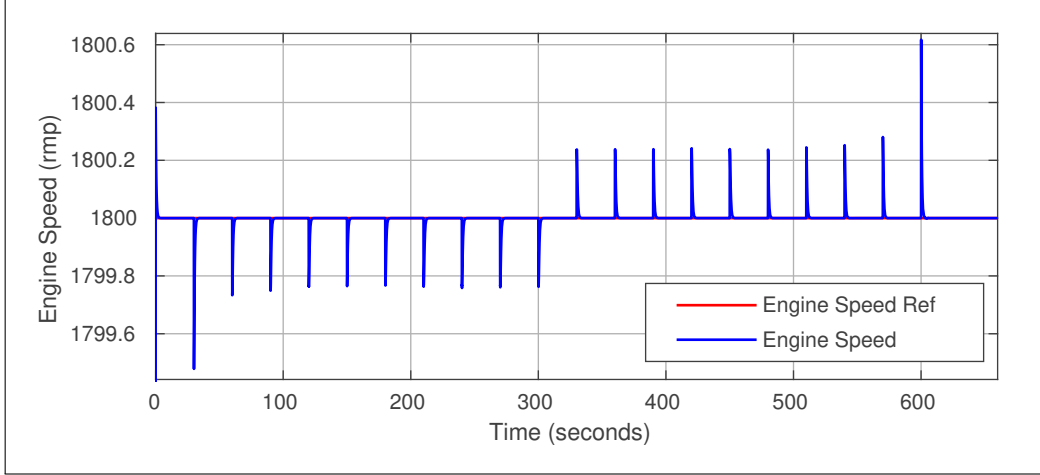


Figure 3.5: Diesel engine speed response to load variations.

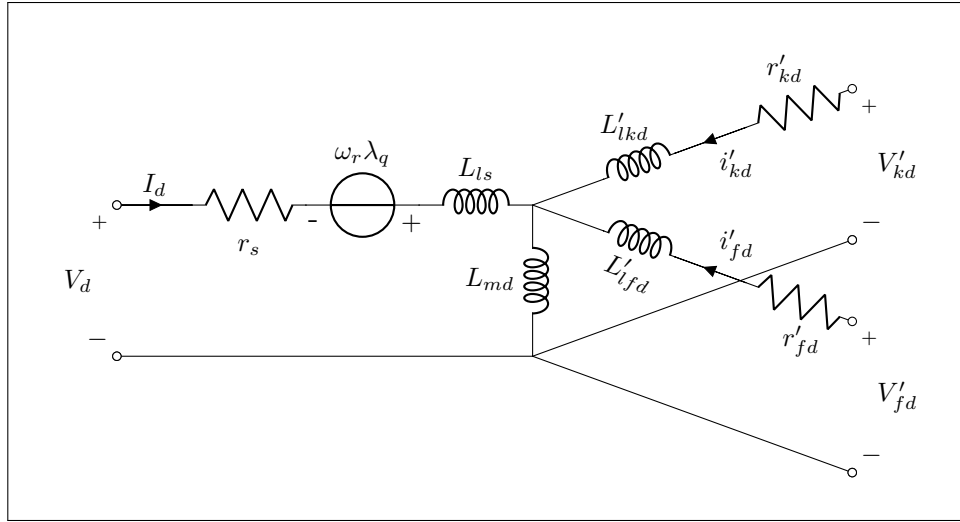
3.2 Synchronous Generator

A synchronous generator is a synchronous machine that converts mechanical energy into electrical energy. A synchronous machine is called so because the frequency of the electric current is synchronized with the rotor. It consists of a rotor with rotor windings that rotates in a stator. The stator windings are connected to the AC mains. Figure 3.6 shows the equivalent circuit for the dq- axis of a three-phase synchronous generator with the reference frame fixed in rotor. The subscripts f and k represent quantities related to the field winding and the damper winding, respectively. The magnetization inductances are shown as L_{md} and L_{mq} .

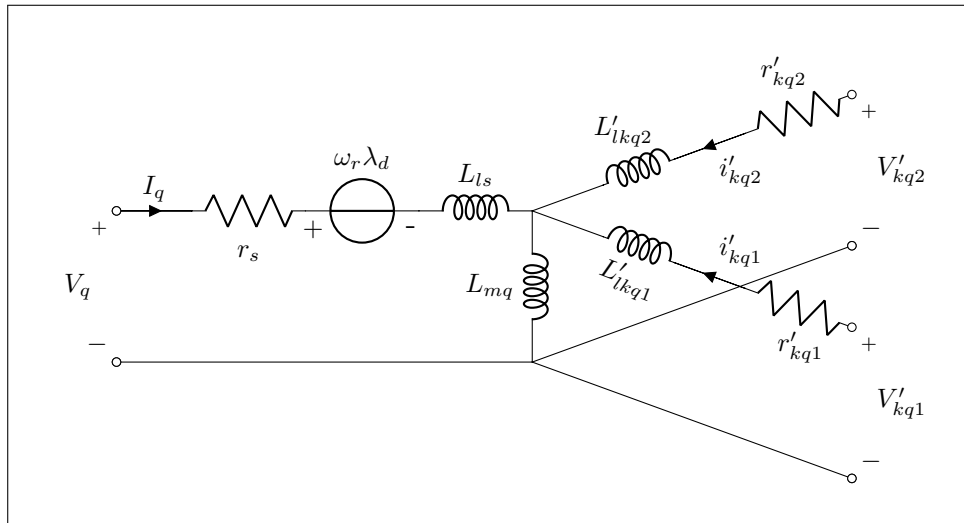
It is convenient to represent the time varying quantities, such as magnetic flux and voltage, in a rotating reference frame that is fixed in the rotor. This transforms the time varying quantities into equivalent DC values. The transformation is described in detail in Chapter 6. Voltage output of the generator in the rotor reference frame for dq axis can be summarized as [15]

$$V_d = r_s i_d - \omega_r \lambda_q + \frac{d}{dt} \lambda_d \quad (3.3)$$

$$V_q = r_s i_q - \omega_r \lambda_d + \frac{d}{dt} \lambda_q \quad (3.4)$$



(a) Equivalent circuit for d-axis.



(b) Equivalent circuit for q-axis.

Figure 3.6: Synchronous generator equivalent circuit in rotor reference frame

where r_s is the stator resistance, i_d and i_q is the axis current, ω_r is the rotor angular frequency, λ_d and λ_q is the flux linkage for d and q axis respectively.

The electromagnetic torque resulting from the generation of electric power is related to the stator currents as

$$T_e = \left(\frac{3}{2}\right) \left(\frac{P}{2}\right) (\lambda_d i_q - \lambda_q i_d) \quad (3.5)$$

where, P is the number of poles.

The synchronous generator is driven by an engine. The library has separate generator models powered by diesel and natural gas engine. Figure 3.7 shows the Simulink model of a generator. The generator simulation model and the succeeding models described in this chapter are developed by Dr. Peter Young. The engine drives a synchronous generator excited by an IEEE recommended excitation system [16]. The synchronous generator produces electromagnetic torque as described in equation 3.5. The generator outputs the total torque and feeds it into the engine block, thus forming a close loop. All the measurements from the engine and the generator are coupled together in separate measurement buses.

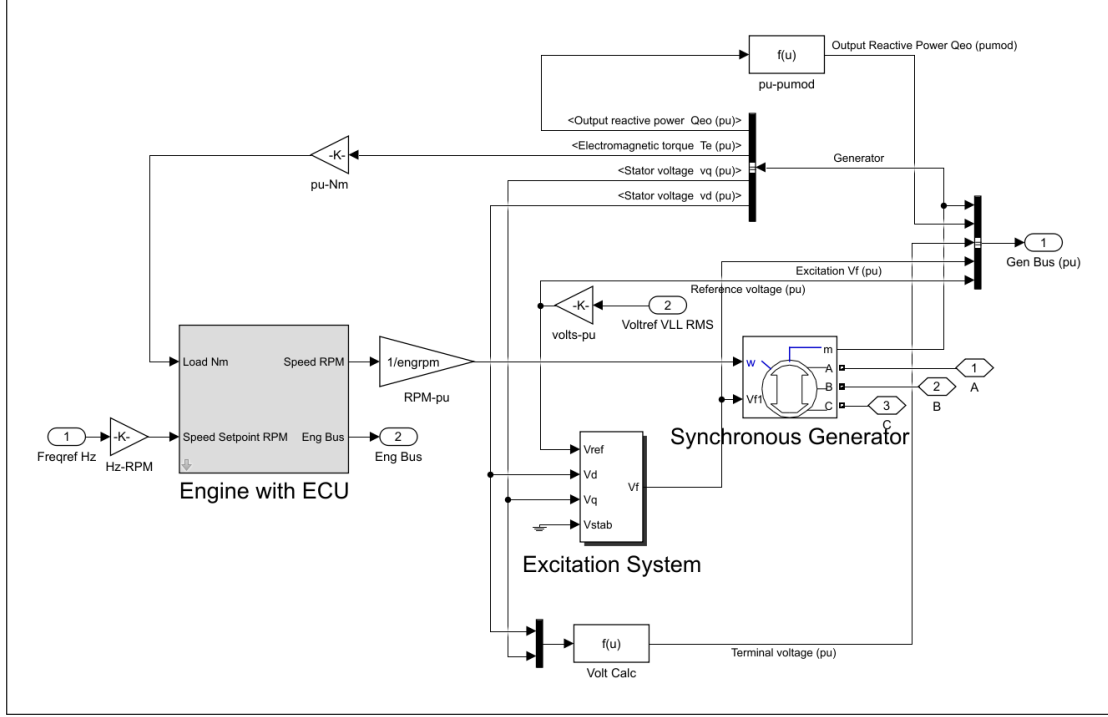


Figure 3.7: Simulink model of Synchronous generator powered by a natural gas engine.

3.3 AC grid frequency control as a power control technique

A generator is essentially a giant rotating spindle. In addition to the electromagnetic torque that is the byproduct of the electric power generation, there is the mechanical torque. The mechanical torque is independent of the electromagnetic torque and is a function of the rotor inertia. The mechanical torque for a generator with rotor moment of inertia J is written as

$$T_M = J \left(\frac{2}{P} \right) \frac{d}{dt} \omega_r \quad (3.6)$$

A torque source, in this case an engine, must overcome the mechanical torque and the electromagnetic torque. Thus, total input inertia to an engine is

$$T_I = T_e + T_M \quad (3.7)$$

Considering equation 3.5, the torque is a function of current. Thus, any increase in the load or increase in power demand would translate to a higher current being drawn. This leads to an increased torque input on the engine. From equation 3.1, for a steady state operation, i.e. constant fuel would mean a decrease in engine rpm. The engine rpm is directly proportional to the AC output frequency. An engine with a speed controller would inject more fuel into the engine to maintain the speed and cope with the increased torque. Thus, maintaining the AC frequency acts as a power control technique in an AC grid.

3.4 Multiple Generator Operation

Microgrids are deployed in varied scenarios with different load requirements. Where a single generator is insufficient to meet the load demand, multiple generators are deployed. The generators act as a single unit servicing the load demand. Over the years, numerous control techniques have been developed to control multiple generation units. The following sections describe two popular multiple generator control techniques.

1. Frequency Droop
2. Isochronous load Share

The mode of operation can be selected from the topmost mask as shown in Figure 1.1b . These operating modes are explained in the next section. The synch control block and the generator breaker are used to synchronize the generators when operating in multi-generator mode.

Droop Control

Frequency and Voltage Droop control are popular control techniques for distributed generation units. Droop control is widely used in the utility power grids to manage and distribute power among various power generation units. The popularity of this technique can be gauged from the plethora of available literature on droop control. The droop control is a decentralized control scheme and is widely popular in application areas where there the cost of a centralized control is very high, or such control is not possible [17].

Droop control is a low-cost load sharing technique implemented using existing grid resources. The load sharing between multiple generator units is achieved within each module by drooping the output frequency as function of generator output power [18].

Generator units that convert mechanical energy into electrical energy have the inherent feature, such that, the power drawn is proportional to the torque on the rotor. The torque, in turn, is proportional to the rotational speed of the engine. Droop technique exploits this feature to achieve load sharing. A droop controller, based on droop curve for individual generator, sets the reference frequency of the generators, thus providing a linear correlation between frequency droop and the load being serviced. Figure 3.8 shows the graphical operation of droop control in two generators G1 and G2. The graph shows the linear relation between the generator power P (when operating alone) vs the output frequency ω . Each generator is evaluated and is assigned a droop curve. A high-power generator would have small frequency variations for an increased load. This would translate to a less steep curve, as evident in the Figure for generator G1 that has a higher output power than G2. All the generation units are connected in parallel to a common AC bus. The AC bus acts as a communication medium. All the generator units continuously monitor the frequency and based on the measured frequency and the droop curve, the controller sets the reference frequency. For example, the reference frequency for a fully loaded generator would be set higher than the actual grid frequency. The generators are preprogrammed with droop control curves, as described in equations 3.8 and 3.9. The load controller injects the bias into the frequency reference using the following formula.

$$bias = f_{gain} \left((f_{set} - f_{meas}) - \left(f_{droop} * f_{rated} * \frac{P_{meas}}{P_{rated}} \right) \right) \quad (3.8)$$

where f_{gain} is the frequency gain, f_{set} and f_{meas} is the set reference frequency and the measured frequency. f_{droop} is the frequency droop for the given generator. f_{rated} is the rated frequency for the system. P_{meas} and P_{rated} is the measured and rated power of the system. The voltage bias to be added to implement the droop is described below.

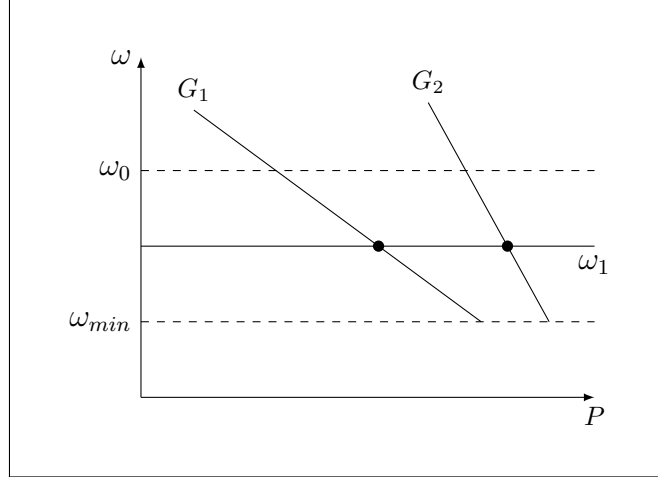


Figure 3.8: Frequency Droop Control for two Generator Units with different max power.

$$bias = V_{gain} \left((V_{set} - V_{meas}) - \left(V_{droop} * V_{rated} * \frac{Q_{meas}}{Q_{rated}} \right) \right) \quad (3.9)$$

where V_{gain} is the voltage gain, V_{set} and V_{meas} is reference and measured voltage, respectively. V_{droop} is the amount of droop for a generator. The amount of droop in absolute terms would be different for each generator based on the it's output power. In terms of percentage the amount of droop is usually same for each generator. V_{rated} is the rated voltage output of the generator. Q_{meas} and Q_{rated} is the measured and rated reactive power of the generator and the system, respectively. Typically, large grids operate at a droop of around 5% [19]. As mentioned previously, a grid controlled using droop technique must be immune to small variations in the frequency. If the generators are synchronized, small frequency variations are absorbed by the grid due to inertia of the rotors. Droop load sharing technique is only applicable where the grid frequency variations due to load changes are small [17].

Isochronous Load Share

Frequency droop control for load sharing among distributed generation units used the existing electrical grid infrastructure as a communication medium. This approach reduces system cost as no modifications to the infrastructure are needed. Other than the cost factor, droop control has many downsides. It assumes the generators have a linear power to frequency relation. Secondly, it

can only work with a slowly varying load. Thirdly, the grid must be able to tolerate slight errors in the actual generator frequency. These above-mentioned factors play a major role in microgrids. The generator size is small as compared to utility grid, thus the prime movers have less inertia. This translates to a nonlinear relation between the generator output power and the frequency. Also, a lower inertia means that any errors in the frequency cannot be overcome. This can greatly reduce the power quality. Also, microgrids usually have to deal with fast varying loads, thus droop control might not work as intended. Microgrids are local installations, thus the cost of a communications infrastructure for a centralized control of the microgrid would be low. In addition to this, there has been a considerable decline in the cost of communications infrastructure, such as wireless mesh networks, or other industry standard bus communication protocols such as CAN or I2C [20] [21].

In an isochronous load share is load sharing control technique the distributed generation units continuously communicate with each other over a communication medium, sharing the grid load information. The generation units send their current power output and receive the overall grid power or load information. The isochronous controller then sets the generator to a set power level proportional to the required grid power demand. This procedure is executed in each of the generators, resulting in a proportional load sharing among all the generators. Thus, the generation units would operate at the same voltage or frequency irrespective of the load [22].

Control blocks inject appropriate bias thus controlling the amount of load share to be assigned based on the actual load information shared over the generator communications bus. The amount of load share for each generator must be determined in advance. The load share is calculated using the known maximum output power of each generator and the maximum load requirement of the system. The load control block computes the frequency bias to be injected into the reference using the underlying formula

$$bias = \left(\left(\frac{lfac}{100} * (P_{avg} - P_{meas}) * P_{gain} * \left(\frac{f_{meas}}{P_{rated}} \right) \right) \right) + \left(\left(\frac{100 - lfac}{100} \right) * (f_{set} - f_{meas}) * f_{gain} \right) \quad (3.10)$$

$lfac$ is the load factor. It is set in the outermost block parameters mask. P_{avg} is the average power output of all the generators combined. P_{meas} is the measured output power of the generator. P_{gain} and f_{gain} are the power and the frequency gain. These determines the gain for the bias controller. f_{set} and f_{meas} are the set reference frequency for the grid and the measured frequency of the generator. The bias calculation for the voltage control block is shown below.

$$bias = \left(\left(\frac{lfac}{100} \right) * (Q_{avg} - Q_{meas}) * V_{meas} * \frac{Q_{gain}}{Q_{rated}} \right) + \left(\left(\frac{100 - lfac}{100} \right) * (V_{set} - V_{meas}) * V_{gain} \right) \quad (3.11)$$

Q_{avg} and Q_{meas} is the average reactive power and the measured reactive power, respectively. V_{meas} is the measured voltage. Q_{gain} and V_{gain} is the gain value for the reactive power and the voltage. Q_{rated} is the rated reactive power for the whole system.

3.4.1 Generator Synchronization

An AC waveform consists of electric quantities that are time varying sinusoids. When multiple generation sources are to be connected to power a single load, the sources are connected in parallel. All the sources must be in phase when the generators are physically connected. Failure to do so might lead to high fluctuating voltages and introduce damaging harmonics in the system, that can cause machine damage etc. Synchronization is a process by which various generation units connect to an AC grid.

A synchronization controller continuously monitors the main AC bus and the output of the generation unit. The sync block measures the two inputs and computes the error. The errors are, the magnitude, phase and frequency. The controller computes these errors and feeds them to three separate PI regulators. The regulators inject control signals or bias to set the reference values for the generator. The regulators would drive the errors to zero. When the errors are within a threshold, the controller sends the command to close the breaker to connect the generator to the bus at which point the synchronization controller for that generator is turned off and regular isochronous or droop control takes over. In a system with inertial power sources such as synchronous generators

powered by an engine or a turbine, small variations in the phase from different sources are absorbed due to the inertia of the grid. Additional figures depicting generator with bias control blocks and synchronization blocks are shown in appendix.

Chapter 4

Photovoltaic Power System

Photovoltaic (PV) cell is a semiconductor device that generates power from the electromagnetic spectrum corresponding to the visible light. The photons in the visible spectrum have enough energy to free electrons in the solar cell. The cell is fabricated using a semiconductor material, such as silicon, that has been selectively doped to create a potential barrier [23]. The freed electrons generated by the photons create a potential difference which is used to drive current through a circuit. A solar cell is the building block of a solar or photovoltaic array.

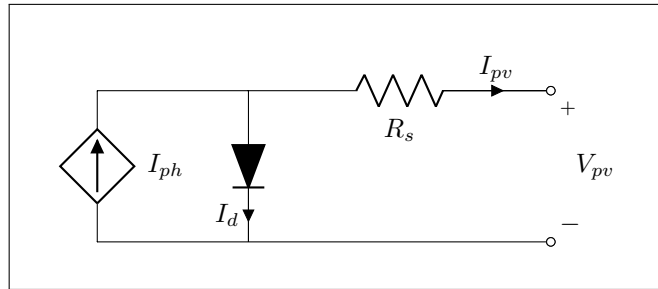


Figure 4.1: Equivalent circuit of a PV cell.

A PV cell is a photodiode that can be modelled using the equivalent circuit depicted in Figure 4.1 (neglecting temperature dependence). Neglecting parallel any resistance in parallel to the current source, the total current output I_{pv} is

$$I_{pv} = I_{ph} - I_d \quad (4.1)$$

I_{ph} is the current generated in the solar cell when illuminated. The current through the diode I_d is modeled as

$$I_d = I_0(e^{(V_{pv} + I_{pv}R_s)/V_T} - 1) \quad (4.2)$$

Where V_{pv} is the diode output voltage, I_0 is the saturation current and V_T is the diode thermal voltage. The thermal voltage is a function of temperature. R_s is the internal series resistance of the cell. Thus, total current, from equation 4.1, [24]

$$I_{pv} = I_{ph} - I_0(e^{(V_{pv} + I_{pv}R_s)/V_T} - 1) \quad (4.3)$$

A typical single PV cell has a power output of a few watts, therefore, multiple PV cells are combined in series and parallel to achieve required output voltage and power. Such an arrangement of PV cells is called a photovoltaic panel.

The PV array simulation block implements an array of photovoltaic cells. The block allows one to model preset PV modules from the National Renewable Energy Laboratory (NREL) System Advisor Model (Jan. 2014) as well as custom defined PV modules [25]. The simulation block is sourced from Simulink Simscape Power Systems, Specialized Technology Library [26].

Figure 4.2 shows the voltage-current characteristics of a PV panel for various solar irradiation values. For a given solar radiation value, the output voltage is a function of the current drawn by the load or vice versa. Total power output of the panel is thus a function of the load impedance. The curve shows the open circuit voltage and the short circuit current on the right and left extremities of the curve, respectively. On the curve (a), one can notice that, for a given value of solar radiation, there is a point on the curve that corresponds to maximum power output. For a load with fixed impedance, the operating point lies somewhere on the curve, that might not correspond the maximum operating point. As the solar radiation fluctuates, the operating point would shift. This leads to a suboptimal solar output if the load impedance is constant.

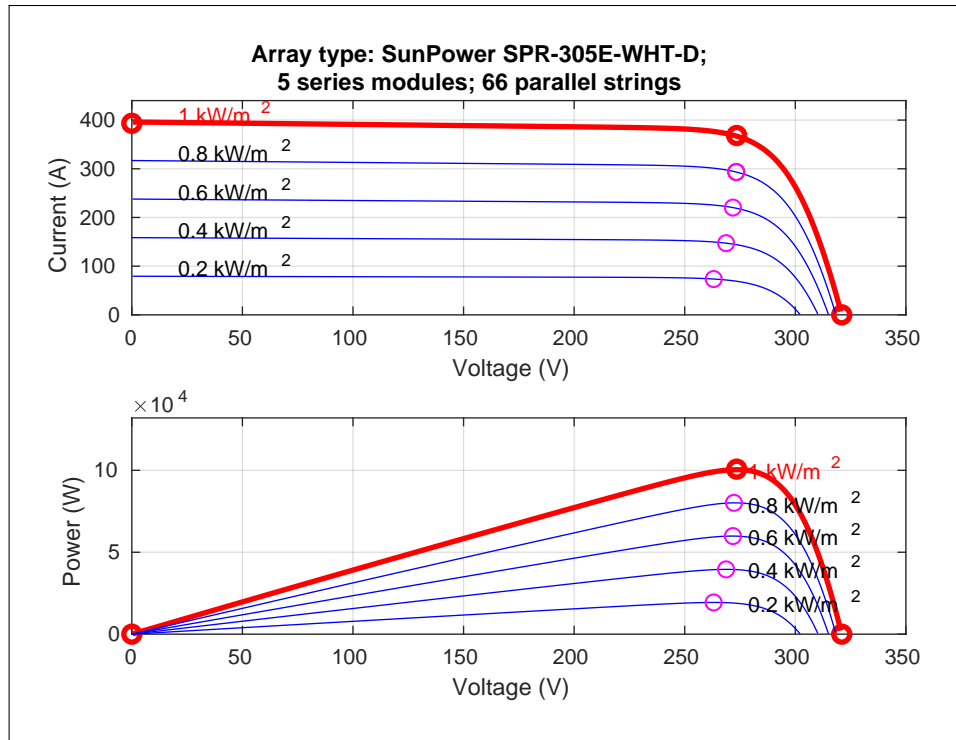


Figure 4.2: Typical voltage current curves for various solar irradiance values.

Changes in solar radiation occur due to sun's movement, any cloud activity or weather event which affects the total solar radiation received by the panel.

4.1 Maximum Power Point Tracking

To extract maximum power output from the PV panel, the voltage and output current of the panel must be controlled. In Figure 4.2, one can notice that, for a given radiation value, the extremities on the graph shows minimum output power. The panel has maximum output power at the knee of the curve, shown as a pink circle. Thus, a controlling device becomes essential that can vary the impedance seen by the PV panel to extract maximum power. This can be achieved by varying the voltage or current drawn from the panel. Such a controller is called a maximum power point tracker, and the underlying technique is called a maximum power point tracking (MPPT) [27].

A popular MPPT technique is called hill climbing or perturb and observe. The perturb and observe algorithm can be summarized as, a change or perturbation of operating voltage of the PV panel would induce a change in the output power, the resulting change in the output power gives the direction of the maximum power point [21]. The MPPT controller controls the duty cycle of a DC/DC converter which will change the current drawn and hence the effective impedance seen by the PV panel.

The algorithm is also called hill climb as the perturbation, if in the direction of maximum power point, is analogous to climbing a hill. The MPPT controller reads the voltage and current from the PV panel. In every execution cycle the controller computes the time rate change of power and voltage. It then checks if the rate of change is negative or positive. For a positive rate of change of power, the controller compares the instantaneous rate of change of voltage. For a positive change, it increases the duty cycle, and vice versa. The opposite happens in the case of a negative rate of change in the power. The step size of the duty cycle is fixed and is determined empirically. A large step size would make the controller responsive but can lead to unstable behavior. A small step size would make the controller sluggish. Modified algorithms have been proposed that use an adaptive or variable step size, and have shown to have improved performance over a fixed step size [28]. The code for the algorithm is described in Appendix A. When the controller reaches the maximum power, it oscillates around that point.

DC-DC converter can be selected based on the requirements of the solar energy harvesting system. The library implements a boost converter. Figure 4.3 shows the schematic of a boost converter.

A boost converter is a switched mode converter that produces DC voltage greater than the input voltage. The main components of a boost converter are, an inductor on the input side, a fully controllable switch in parallel. The switch is a semiconductor switch, such as a MOSFET. Diode D_1 acts as a unidirectional switch. A capacitor is added at the output stage to filter out the ripple and smoothen the output.

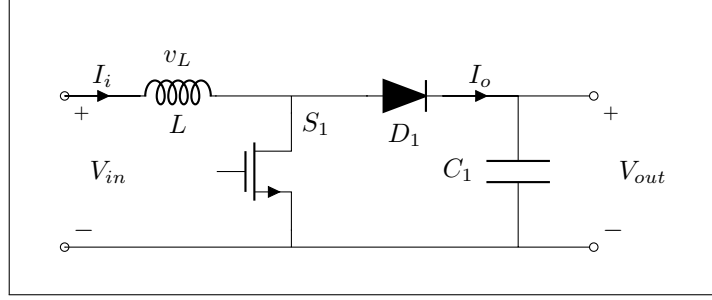


Figure 4.3: Boost converter.

A boost circuit can be analyzed using the small ripple approximation [29]. The switch S_1 is driven by a controller that feeds a square wave of frequency f and duty cycle D . The converter operates in two states, state one when the switch S_1 is closed and state two, when the switch is open. In state one, the input voltage V_{in} equals the voltage drop across the inductor.

$$V_L = V_{in} \quad (4.4)$$

Given the time period of the square wave is T_s , total time the converter is in state one is, DT_s , where D is the duty cycle.

In state 2, the switch is open, thus the current flows through the diode D_1 . This results in the voltage across the inductor and the input voltage to be in series. Inductor voltage in state two is

$$V_L = V_{in} - V_{out} \quad (4.5)$$

The converter is in state two for $(1 - D)T_s$ seconds. Total volt-seconds applied to the inductor over one switching interval are

$$\int_0^{T_s} V_L dt = (V_{in})DT_s + (V_{in} - V_{out})(1 - D)T_s \quad (4.6)$$

Equating the term to zero and simplifying, the output voltage for a boost converter is related to the input as

$$V_{out} = \frac{V_{in}}{1 - D} \quad (4.7)$$

which gives voltage boost since $0 < D < 1$.

The MPPT controller varies the output voltage by controlling the duty cycle thereby controlling the output power. The boost converter implemented in the library is an average characteristics model that does not simulate the switching devices. The switching devices are replaced by voltage and current sources. Different power electronic component modeling techniques are described in section 7.2.1.

Figure 4.4 shows the Simulink implementation of the PV module, MPPT controller and the DC-DC converter. Simulation setup is derived from Examples for Simulink Simscape Power Systems, Specialized Technology. The DC-DC converter is an average characteristics single quadrant boost converter model sourced from Sim Power Systems, IREQ, Power Electronics Library [30]. The following section illustrates the working of an MPPT controller by comparing a PV panel controlled by an MPPT controller and the other connected to a constant load without an MPPT controller.

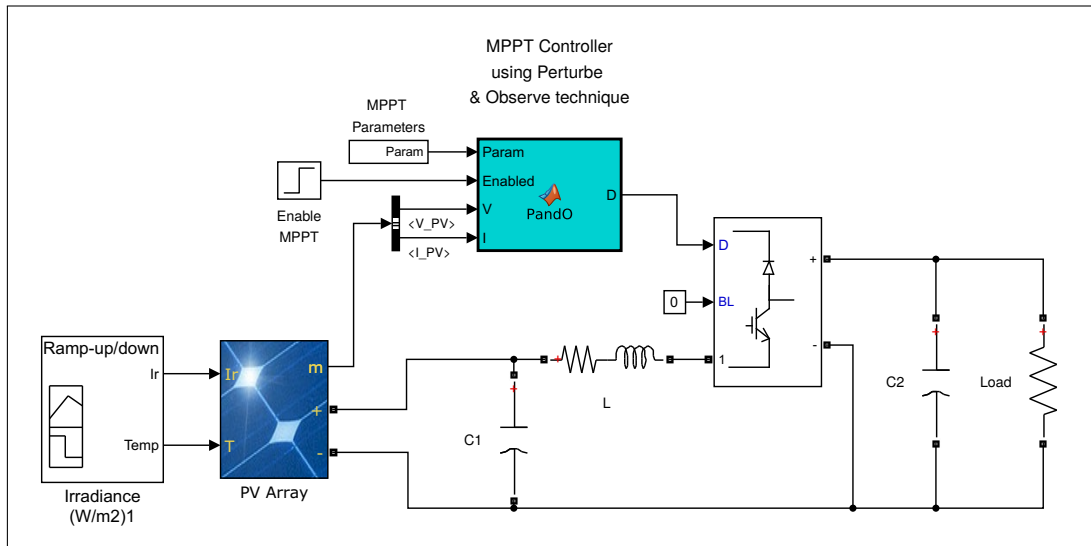
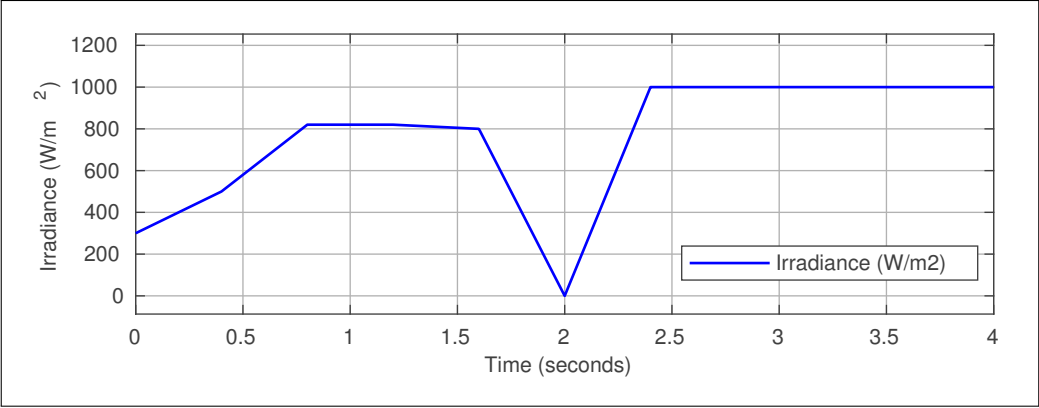


Figure 4.4: PV panel block with an MPPT controller simulation in Simulink.

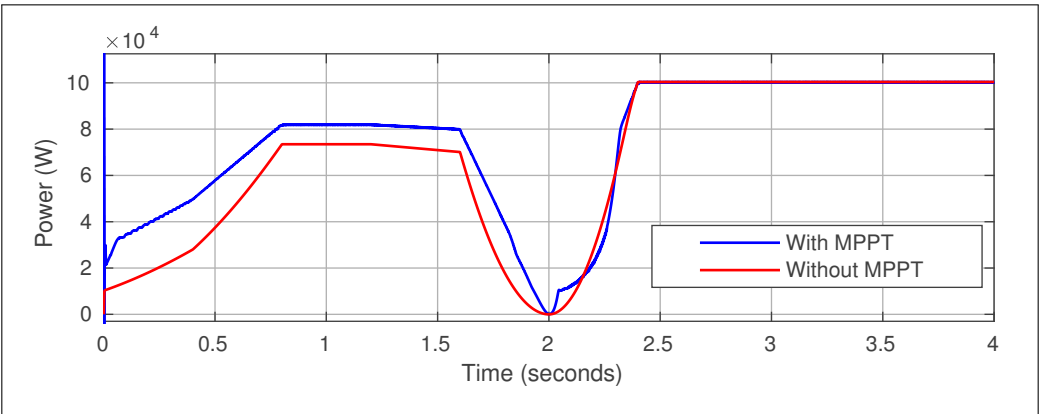
To illustrate the working of the MPPT controller, the PV panel in the two setups is irradiated with similar solar radiation profile shown in Figure 4.5a. Referring to Figure 4.2, the maximum power point, for solar irradiation of 1000 w/m^2 , occurs at a voltage of 273 V. Maximum power at this point is $1.007 \times 10^5 \text{ W}$. The corresponding impedance for maximum power is 0.74Ω

In the first setup, the PV panel is connected to a DC/DC boost converter controlled by an MPPT controller. The controller is connected to a load with an impedance of 100Ω . In the other setup, the PV panel is connected to a load with an impedance of 0.74Ω . This corresponds to the maximum power point for irradiation of 1000 w/m^2 .

Figure 4.5b shows the power output from a PV panel, with and without an MPPT controller. For solar radiation value less than 1000 w/m^2 , the MPPT controlled PV panel shows a higher power output than the constant impedance load. This illustrates that at suboptimal load, the MPPT controller adjusts the duty cycle, extracting maximum power from the panel. The constant impedance load is optimized to represent maximum power output at maximum irradiance. This is evident from the power output for solar irradiance levels of 1000 w/m^2 . The MPPT controller adjusts the panel output to match it with the power output for the optimal load impedance.



(a) Solar irradiance profile.



(b) Power output from two similar solar panels, with and without an MPPT controller.

Figure 4.5: Power output with and without MPPT controller.

Figure 4.6 shows the plot of output power vs panel voltage for a solar panel controlled using an MPPT controller. The power output is superimposed on the power curves corresponding to various solar irradiance values. Maximum power for a given solar irradiance occurs at the tip of the curve. Notice that the MPPT controller tracks the maximum power resulting from changes in the irradiance. This is shown as a zigzag tracking curve that follows the tips of the power curves.

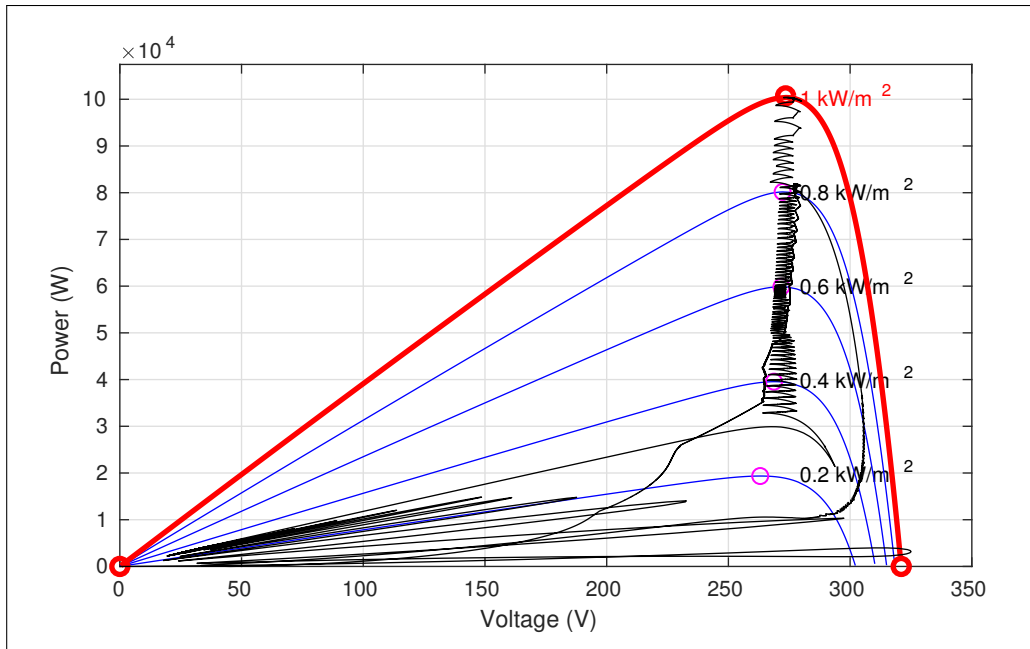


Figure 4.6: PV panel power output superimposed on the power curves for various irradiance values.

Chapter 5

Battery Storage System

Grids relying on renewable sources of energy such as wind and photovoltaics require some form of energy buffer. The energy buffer helps to overcome fluctuations in the power output from these sources. The buffer, thus, stabilizes the output to provide a consistent power. Battery banks have been successfully employed in large grids to meet power demands in peak hours. Battery banks are not widely employed because of high investment cost and the issue of economic feasibility. One important characteristic of the battery is that, it is an instantaneous energy source. Energy can be stored in the battery during the charge cycle, when the load demand is low. This stored energy can then be harnessed when needed during high demand. This property of the battery is utilized in microgrids. It acts as an on demand energy source to provide the much necessary power to overcome transients.

There are numerous battery storage technologies currently in use. Battery technology refers to the underlying chemistry of the battery and the material composition. Until the recent past, the preferable choice of battery technology has been the lead acid battery. It has a fairly constant voltage operation, and is economical. Another battery type that has been gaining a lot of momentum is the lithium-ion battery. Li-ion batteries has the largest energy density and close to 100% storage efficiency compared to all the other commercial battery types [31]. Increasing demand and improvement in manufacturing techniques has lead to decrease in the price and an increase in the energy density. Thus, Li-ion batteries make an ideal choice to act as an energy buffer in a microgrid.

The next sections describe the battery model, the charge sequence for a lithium ion battery and the battery controller, respectively.

5.1 Battery Model

The Simscape Power Systems, Specialized Technology library has a battery model that can simulate various types of batteries [32]. Battery discharge is modeled using

$$f_{discharge}(it, i^*, i) = E_0 - k \frac{Q}{Q - it} \cdot i^* - K \cdot \frac{Q}{Q - it} \cdot it + A \cdot r^{-Bit} \quad (5.1)$$

where E_0 is the constant voltage, K is polarization constant (units in Ah^{-1}), i^* is low frequency current dynamics (units in A), i is the battery current, it is the extracted capacity (units in Ah or C), Q is maximum battery capacity (in Ah), A is exponential voltage, and B is the exponential capacity. Battery charging is modeled using the following equation

$$f_{charge}(it, i^*, i) = E_0 - k \frac{Q}{0.1Q + it} \cdot i^* - K \cdot \frac{Q}{Q - it} \cdot it + A \cdot r^{-Bit} \quad (5.2)$$

Nominal voltage is defined in terms of the discharge characteristics. Discharge characteristics of a battery are evaluated by discharging the battery at constant current. Nominal voltage is the battery voltage at the end of the linear voltage response when discharging at constant current. Figure 5.1 shows the discharge curves for a lithium-ion battery at various discharge currents, obtained using plotting function in the battery model. Battery specifications are listed below.

Table 5.1: Li-ion battery specifications.

| Specifications | Details |
|-----------------------|--------------|
| Battery Capacity | 2.3 Ah |
| Nominal Voltage | 3.22 Ah |
| Fully Charged Voltage | 3.7 V |
| Internal Resistance | 10m Ω |

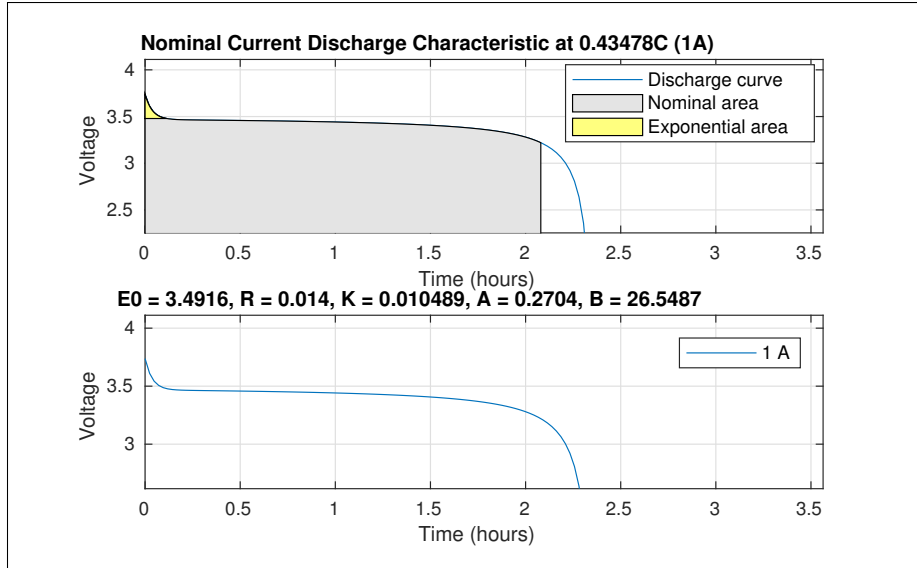


Figure 5.1: Discharge curve for the battery.

5.2 Battery Controller

A lithium-ion battery has stringent charge requirements. Failing to meet these might result in permanent damage to the battery [33]. This necessitates that a battery be connected to the application circuit via a battery controller.

5.2.1 Lithium-ion Battery Charging Algorithm

Figure 5.2 shows the typical charging sequence in a lithium ion battery [34]. The charging sequence starts with the charger acting as a constant current source. In constant current mode, there is an increase in battery voltage and state of charge. The controller constantly monitors the terminal voltage and when it reaches a reference value, the controller switches from constant current mode to constant voltage mode. The reference value is determined from the battery datasheet and it corresponds to battery voltage at full charge. In constant voltage mode, the battery terminal voltage is held at a constant value. This results in decreasing battery current. Lithium-ion batteries are sensitive to overcharging. To prevent overcharging, the controller monitors the battery state of charge and the charging is terminated when the state of charge reaches 100%.

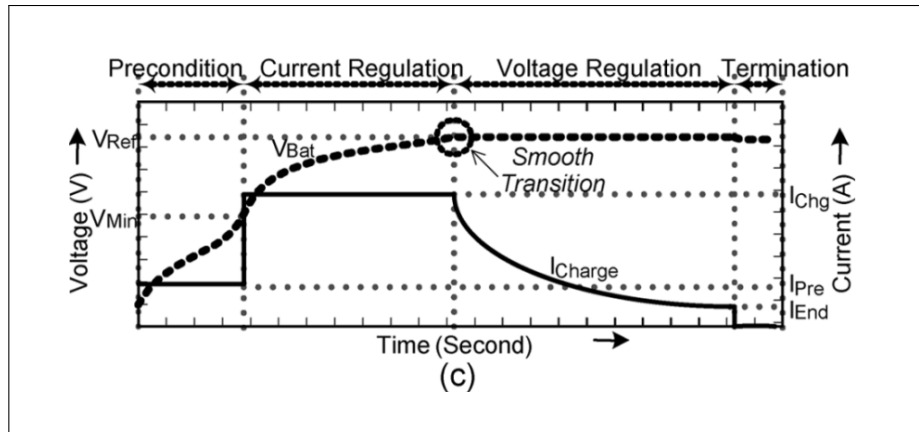


Figure 5.2: Lithium-ion battery charging sequence.

5.2.2 Battery Controller Implementation in Simulink

Figure 5.3 shows Simulink implementation of the battery controller. The controller consists of a battery controller block that contains the control system and a controller function block. The controller function block is responsible for selecting the appropriate controller operation mode. The controller commands a control output 'D' (Duty cycle) that controls a buck-boost (two quadrant DC/DC) converter. The converter block is sourced from Simulink Simscape Power Systems, Specialized Technology Library. The two-quadrant DC/DC converter is setup in current control mode. The battery controller block lets user select way the battery acts, either as a constant voltage source or constant current source.

Figure 5.4 shows the battery controller block. The two quadrant DC/DC converter is setup in current control mode. Based on the selected mode of operation, the controller generates a reference current that is fed to the current regulator.

In constant voltage source mode, the battery controller acts as a constant voltage source when discharging. During the charge cycle, the controller charges the battery using the charging cycle described in Subsection 5.2.1. The charging algorithm states that the controller should transition from constant current mode to constant voltage mode, when the battery terminal voltage exceeds a set reference value. This transition is implemented by a selector switch that selects the appropriate reference current value ' I_{ref} '. Control structures that implement such switching suffer from abrupt

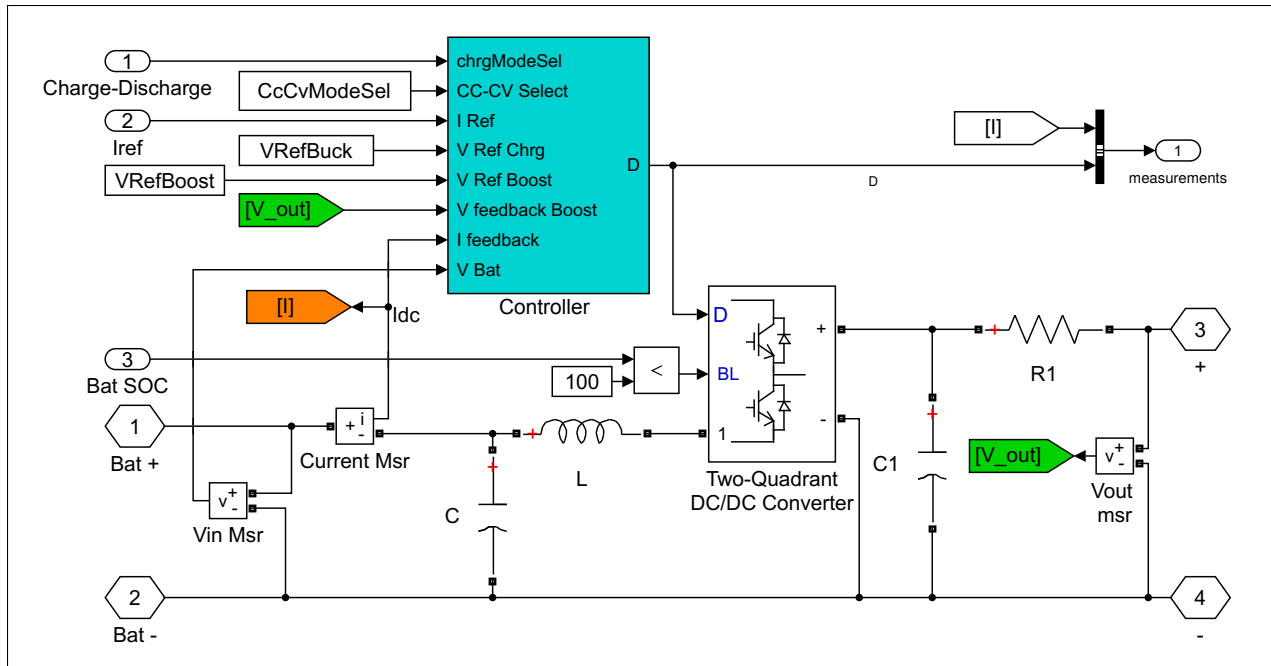


Figure 5.3: Battery controller with converter Simulink implementation.

change in the control output, that shows up as a bump in the controller output. The reason for this abrupt change is because the controller that takes over the control is not tracking the controller output. This results in the controller integrator value to saturate or deviate resulting in a different control output. Such a scenario is avoided by implementing a bumpless transfer of control implemented by tracking the output [22]. Tracking is implemented in the ‘Voltage Regulator Charging’ block shown as an input port ‘TR’.

As a constant current source, the user has the option of implementing a custom current controller that sets the reference current. Sign of the reference current determines the battery charge or discharge mode. Figure 5.5 shows the controller GUI and the parameters mask with the parameter fields.

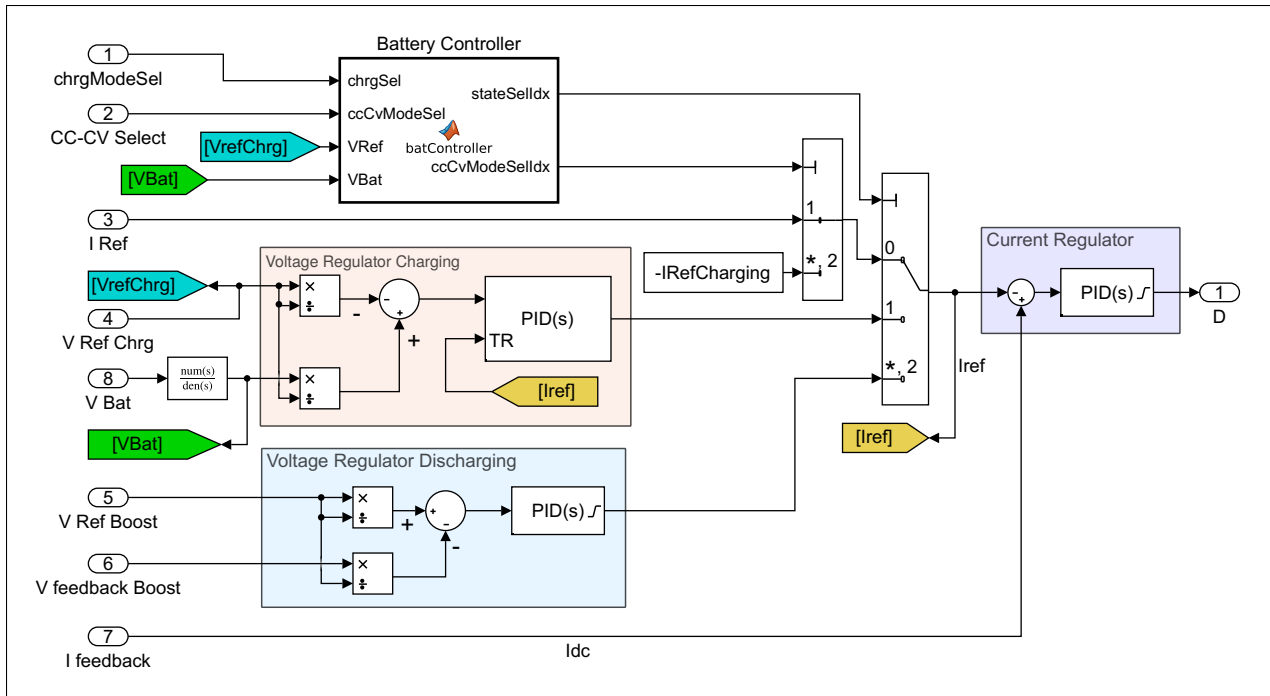


Figure 5.4: Battery controllers.

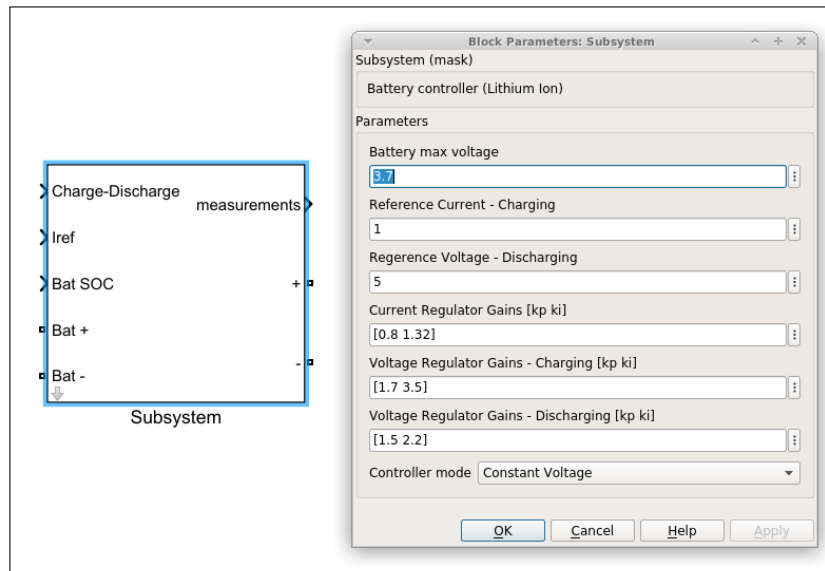


Figure 5.5: Battery controller GUI with the parameters mask.

The battery controller was verified on an A123 lithium-ion battery model. Battery specifications were described in Table 5.1. Figure 5.6 shows the battery voltage during the charge cycle. The battery is charged in the constant current mode at the rate of 1 C. Notice the increase in the

battery voltage as the charging progresses. When the battery voltage reaches the fully charged voltage, the controller switches from constant current mode to constant voltage mode. This results in a flat curve as the voltage is held constant. The battery continues to draw current and the state of charge keeps on increasing until it is fully charged. At that time, the controller disables the charging.

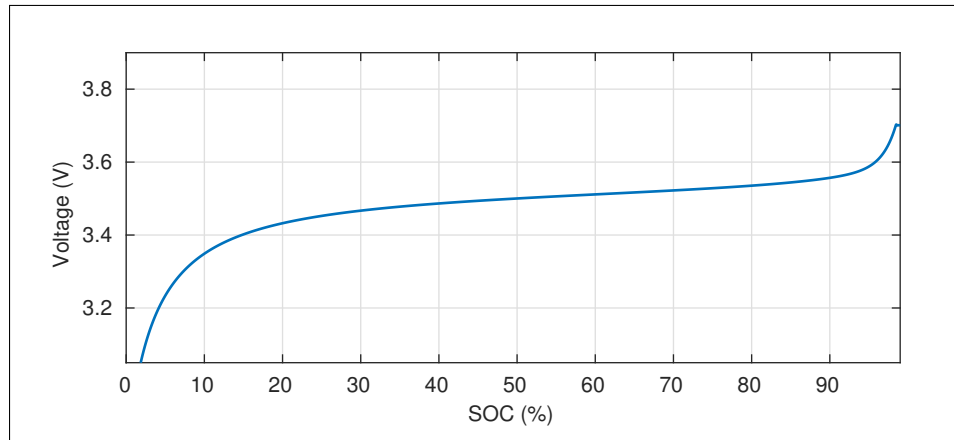


Figure 5.6: Battery voltage vs SOC during charge cycle.

The State of Charge (SOC) of the battery is an important measurement. It determines the actual capacity of the battery. In a physical system, one does not have the information about the internal chemistry of the battery. Thus, the state of charge must be determined from measurable quantities, such as, instantaneous voltage, current etc. Various techniques have been proposed and developed to determine actual state of charge [35] [36] [27]. The battery simulation model in the Sim Power Systems library computes the state of charge using equation 5.2.

Chapter 6

Universal Bridge Converter

Microgrids are designed so that they can be deployed to work with existing electrical infrastructure. Modern electrical infrastructure and electrical appliances are built around the AC grid. PV and battery sources as described in previous sections are DC power sources. Thus, a DC to AC converter becomes an essential component of a microgrid. Microgrid topology like the one described in Chapter 2, section 2.1, require a unidirectional power flow, while some microgrid topologies, like the one described in section 2.2, require a bidirectional power flow. Thus, a converter topology that fulfills the above criteria is the three-phase bridge converter.

The library is targeted towards research into microgrids, thus, the user must have the flexibility to implement different types of configurations. Keeping this in mind, the library was developed so as accommodate different types of implementations that a researcher might encounter. The chapter describes the reference frame theory, three-phase bridge converter and the bridge converter control techniques, respectively.

6.1 Reference frame theory and direct quadrature zero transformation

In a three-phase system, the electrical quantities are sinusoids that are functions of rotor position. Thus, these quantities continuously vary with time, making their analysis difficult. A change of variables can be used to reduce the complexity. This change of variables is a transformation of quantities from one reference frame to other. By selecting appropriate reference frame, one can eliminate all the rotor position-dependent quantities and replace them with equivalent DC type quantities. This type of transformation greatly simplifies the analysis and control of three phase systems.

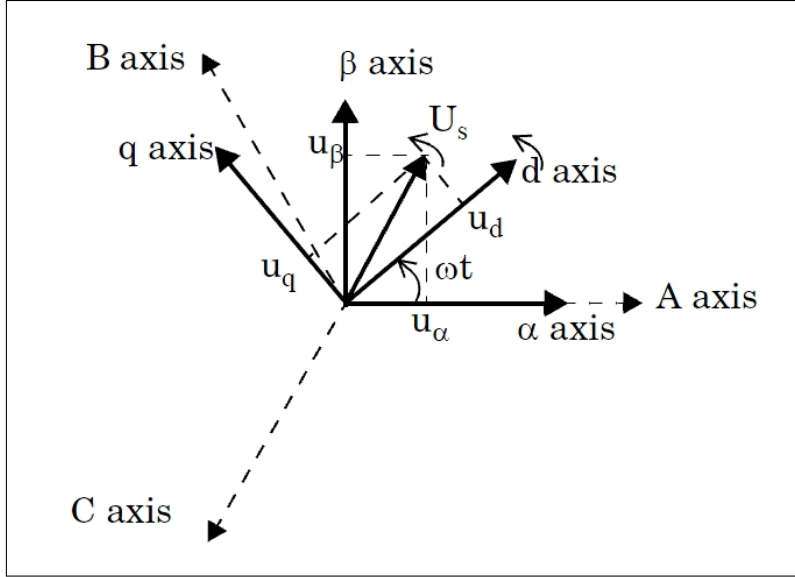


Figure 6.1: ABC to dq0 transformation.

One of the widely used transform is the direct-quadrature-zero or ‘dq0’ transformation. Figure 6.1 shows the ABC axis along with the dq0 axis. The dq0 transform is the product of the Clark transform and the Park transform [37]. The Clark transform converts the ABC vectors to the XYZ reference frame (also called the $\alpha\beta 0$). The ABC vectors can represent any electrical quantity viz. current or voltage etc. The Clark transform used is described in equation 6.1.

$$\mathbf{K}_c = \begin{bmatrix} 1 & -\frac{1}{2} & -\frac{1}{2} \\ 0 & \frac{\sqrt{3}}{2} & -\frac{\sqrt{3}}{2} \\ \frac{1}{2} & \frac{1}{2} & \frac{1}{2} \end{bmatrix} \quad (6.1)$$

The advantage of this transformation is that the three sinusoids are reduced to a single non zero value. The y and the z axis are reduced to zero, thus simplifying the calculations. This is a power variant form because the transformation matrix is not unitary. In this transformation, the q axis leads the d axis as shown in Figure 6.1.

The Clark transform converts the ABC vectors to XYZ, but because the vectors are a function of the rotor position, they still vary with time. To convert the time varying quantities to DC type values, one needs to rotate the XYZ frame at the angular velocity of the rotor. The angle of rotation

of the frame θ , is replaced by the product of angular velocity of the rotor and the instantaneous time. Park transform which is described below.

$$\mathbf{K}_p = \begin{bmatrix} \cos(\theta) & \sin(\theta) & 0 \\ -\sin(\theta) & \cos(\theta) & 0 \\ 0 & 0 & 1 \end{bmatrix} \quad (6.2)$$

The dq0 transform is a Clark transformed reference frame rotating at an arbitrary angular velocity. The dq0 transformation matrix is:

$$\mathbf{K}_{dq0} = \mathbf{K}_p \mathbf{K}_c = \frac{2}{3} \begin{bmatrix} \cos(\omega t) & \cos(\omega t - 2\pi/3) & \cos(\omega t + 2\pi/3) \\ -\sin(\omega t) & -\sin(\omega t - 2\pi/3) & -\sin(\omega t + 2\pi/3) \\ 1/2 & 1/2 & 1/2 \end{bmatrix} \quad (6.3)$$

where ω is the angular frequency of the rotor or the frequency of the AC grid, and t is the instantaneous time. The AC quantities are computed in the reference frame rotating at the instantaneous voltage angular frequency, ω . This eliminates all the time varying quantities, thus transforming them into equivalent DC values. In Simulink, the dq0 transform is implemented using the dq0 transform block [38].

dq0 transform simplifies the measurement of reactive power in the system. To measure the reactive power, hence, the relative phase shift between the voltage and current, the currents in the three phases are computed in the same rotating reference frame as the voltages. The relative phase shift, that corresponds to reactive power in the system, shows up as a non-zero value for the q component. This property is exploited in converter control and is described in detail in section 6.3.

6.2 Three-phase Bridge Converter

A three-phase two level bridge converter consists of six semiconductor devices. These semiconductor devices can be bipolar junction transistors (BJT), insulated bipolar junction transistors (IGBT), metal oxide semiconductor field effect transistor (MOSFET), or any other force com-

mutated semiconductor switch. IGBT and MOSFET are widely used in high power converters because of their superior electrical characteristics. Figure 6.2 shows the schematic diagram of a three-phase bridge converter.

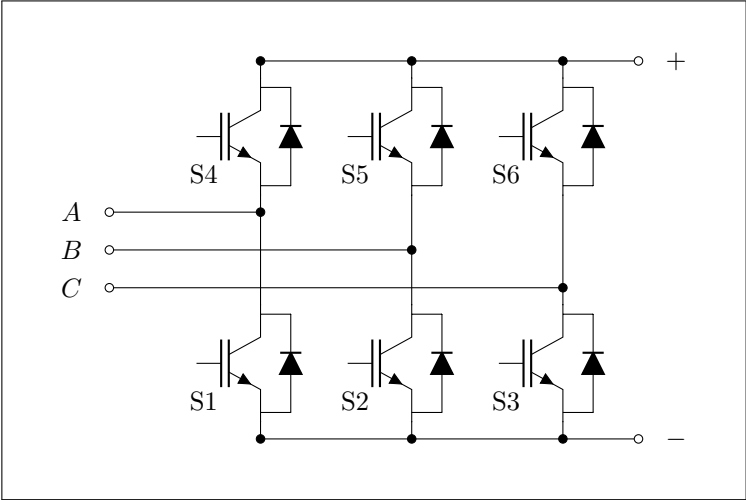


Figure 6.2: Three-phase bridge converter.

Each switch has a blocking diode connected in parallel. A diode is a unidirectional line commutated semiconductor device that only conducts electricity in one direction. The switches are only operated in the saturation or cut-off region to minimize power losses due to heating [15]. Three-phase bridge converters are force commutated converters that require external control of the semiconductor switches. The six switches are fired in a specific sequence with varying lengths of the rectangular switching pulses. This type of waveform generation is called pulse width modulation. Popular pulse width modulation techniques for bridge converters are, carrier based pulse width modulation and space vector pulse width modulation.

Simulink allows users to simulate power electronics devices using different simulation techniques. These simulation techniques are described in Subsection 7.2.1. Simulations and control tools are modeled using average characteristics models that do not model switching waveforms and harmonics.

The next three sections describe the implementation of a three-phase bridge converter as an AC to DC converter and as a DC to AC converter. The sections describe the underlying control technique and then describe the library implementation of the same. Staying true to the objectives of the library, the implementation of the control algorithms is highly flexible. The projected implementation of the controller is, to use the bridge converter as a universal converter. Thus, a supervisory controller must have the ability to switch the control algorithm, and therefore the direction of flow of power.

6.3 Three-phase bridge converter as a PWM Rectifier

A rectifier or an AC to DC converter is a device that converts AC power to DC power. The simplest three phase rectifier comprises of six diodes arranged as shown in Figure 6.2 (neglecting the semiconductor switches). The diodes are line-commutated devices that does not require external control for their operation. The turn-off conditions are determined by the voltages of the AC supply line. Such a rectifier is an uncontrolled rectifier because one does not have control over the output voltage or the quality of the output power.

A Force commutated rectifier is a three-phase bridge converter that is built using a bridge converter constructed using force commutated semiconductor switches. Force commutated rectifiers are also called PWM rectifiers. These are of two types, current-type and voltage-type PWM rectifiers. The library implements a voltage type rectifier because of its superior dc output characteristics [39]. The library uses the average characteristics model based three-phase two-level power converter, sourced from the Sim Power Systems, Power Electronics Library [40]. There are various PWM rectifier control techniques. These can be broadly categorized into: rectifier control in stationary reference frame and control in a rotating reference frame. In a stationary reference frame, the instantaneous electrical quantities such as the voltage, current, magnetic flux, etc are sinusoids. A sinusoidal control has a poor transient response and is prone to steady state errors. Contrary to this, sinusoids in a rotating reference frame are transformed into DC quantities making

the control simpler. Thus, rectifier control is implemented in a rotating reference frame has better steady state and transient performance than in stationary reference frame [41].

There are various control techniques for control of rectifiers in a rotating reference frame [45]. The library implements the voltage oriented control (VOC) technique. The voltage oriented control is based on the unity power factor condition.

6.3.1 Unity power factor condition

In an AC power system, complex power \vec{S} is defined as

$$\vec{S} = \vec{P} + i\vec{Q} \quad (6.4)$$

where \vec{P} is the active or real power and \vec{Q} is the reactive or imaginary power. Power factor is defined as the ratio between real power and complex power, or the cosine of the angle between voltage and current. Power factor gives a measure of the amount of reactive power in the system. A purely reactive system would have a power factor of zero, and a purely active system with resistive elements would have a power factor of unity.

$$Power\ Factor = \cos\phi = \frac{\vec{P}}{\vec{S}} \quad (6.5)$$

Figure 6.3 shows the dq0 transformation for a three phase AC system in the rotating reference frame. The dq0 transformation for the voltages has a nonzero d component V_d , and a zero q component V_q . The dq0 transformation for the AC current is performed in the voltage reference frame. Thus, any reactive components in the circuit will lead to a phase difference in the voltage and current. This phase difference shows up as a non-zero q component in the dq0 transformation of the three-phase AC current. The total current component shows up as I_0 in Figure 6.3.

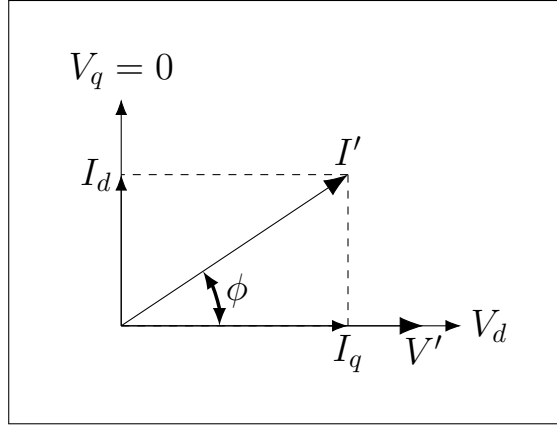


Figure 6.3: Voltage and current axis in dq0 reference frame.

In a unity power factor condition, $\phi = 0$. This condition can only be met if the I_q component equals zero thus aligning the two vectors, I' and V' . This technique is used in the control of three-phase bridge converters [39]. The controller forces the $I_q = 0$, thus ensuring real power is drawn on the AC side.

6.3.2 Rectifier Control

A rectifier can be visualized as a resistive element in the AC grid that absorbs real power, i.e. the d axis is constant and negative, whereas the q axis is set to zero. Figure 6.4 shows the control schematic for a constant voltage three-phase bridge rectifier. Measured AC current I_{abc} is transformed into dq0 axis rotating in the voltage reference frame. The measured I_d and I_q are fed to the respective controllers.

The bottom section shows the controller for the d axis. As a constant voltage source, the voltage controller compares the measured DC voltage with the reference DC voltage. Notice that the feedback is setup so that the controller output is negative. The controller output acts as a reference to the I_d controller. Negative d axis ensures the bridge converter acts as a rectifier, pulling or absorbing real power. Output from the d axis controller generates the control output U_d^* that is fed to a dq0 to abc reference frame transformation block.

For the control of q-axis, the reference I_{qref} is set equal to zero. The error is fed to a PI regulator that generates a control output, U_q^* . The dq0 to abc transformation block transforms the dq control signals into the abc reference frame, shown as U_{ref} . Simulink implementation of the controller is shown in later Figure 6.9.

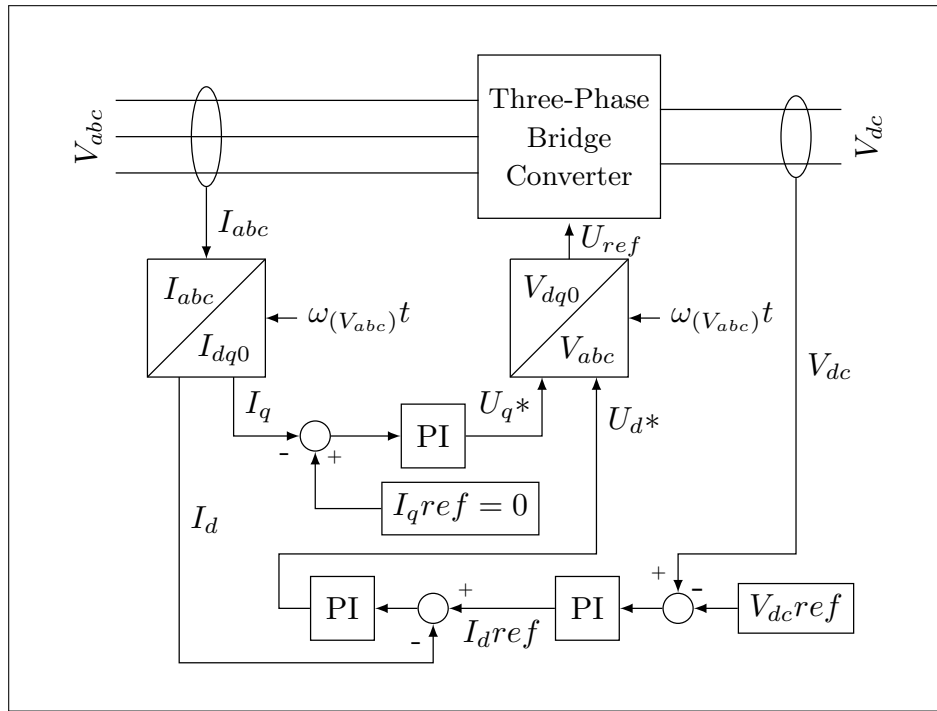


Figure 6.4: Control Structure for a PWM rectifier (Constant Voltage Source).

Figure 6.5 shows measurement from the simulation of a rectifier setup as in constant voltage output mode. The system setup is as follows: AC Line-Line VRMS = 260V, Rectifier output voltage reference = 500V, DC Load impedance = 20 Ohms. Figure 6.5.(a) shows the DC reference voltage and the measured output voltage. The rectifier control reaches the desired reference value.

Figure 6.5 (c) and (d) shows the measured d and q axis for the current. Notice in Figure 6.5(c), the reference for the d axis is set as a negative value. This corresponds to the converter acting as a rectifier, pulling power out from the AC grid. The measured value settles to a steady state in under 0.1 secs. The values are in per unit (p.u.) system. The q axis component reference is set at

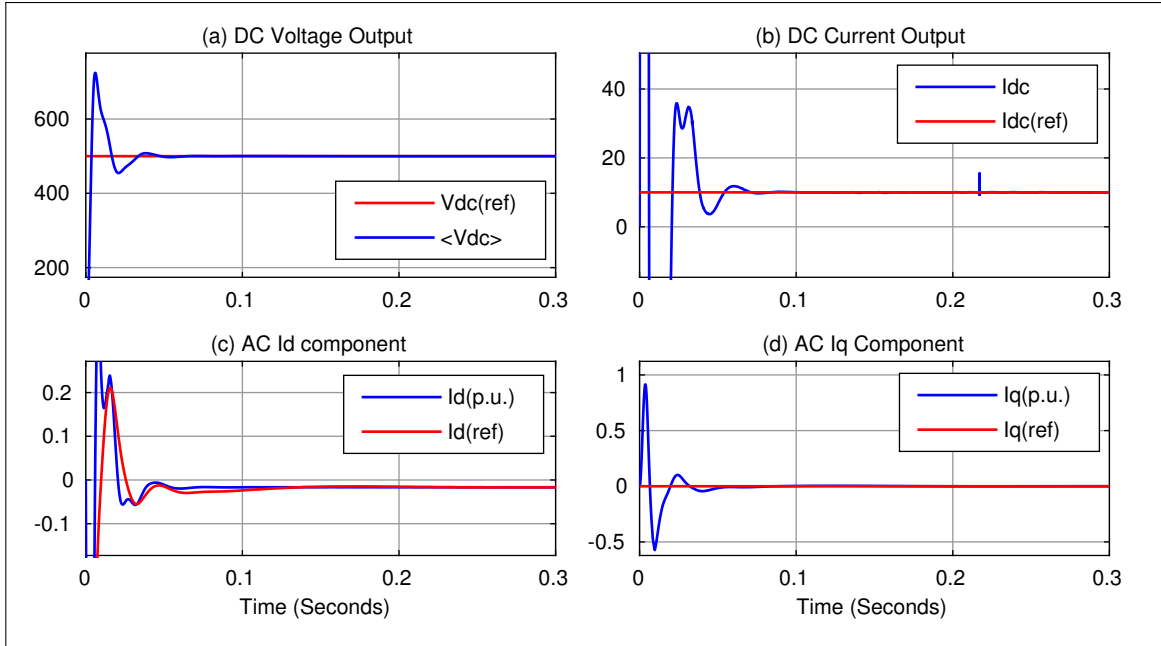


Figure 6.5: Rectifier Output Voltage and Id, Iq axis controller output.

zero. The measured value reaches the reference steady state thus satisfying the unity power factor condition.

6.4 Three-phase bridge converter as a grid forming inverter

A grid forming inverter is employed in microgrid topologies where the inverter acts as the frequency master [11]. In the microgrid topology depicted in Figure 2.1, all the sources feed power into the DC bus. Thus, the inverter acts as the primary AC power source.

In the utility grid, a prime mover such as, a gas turbine is the source of mechanical energy. The mechanical energy from the rotating shaft, connected to a generator, generates the AC power. That rotation of the armature is the source of AC frequency. In an isolated grid, the power is derived from DC sources, thus an inverter must synthesis its own frequency. A clock source in the inverter controller generates the required reference frequency.

6.4.1 Inverter Control

For a grid forming inverter, there are two major control objectives. First one is to maintain the output AC voltage at the desired reference value. Second objective is to maintain the grid frequency. A controller in the stationary reference frame would view the inverter output as sinusoids. PI controllers are known to have poor steady state performance for sinusoidal signals. Therefore, the controller is implemented in a rotating reference frame, transforming the sinusoids into equivalent DC values. The AC output is transformed into the dq0 reference frame.

An inverter can be visualized as a power source that injects real power into the system. In the dq0 reference frame, the d axis for an AC voltage is a positive value, and the q axis is zero.

Figure 6.6 shows the controller schematic for a grid forming inverter. All the values are in p.u. system. A clock source generates the reference grid frequency signal. The reference frequency is shown as an input to the dq0 to abc transformation block. The reference signal is inverse Park transformed to abc reference frame. The generated reference output is fed to a Space Vector Modulator that triggers the semiconductor devices in the bridge converter.

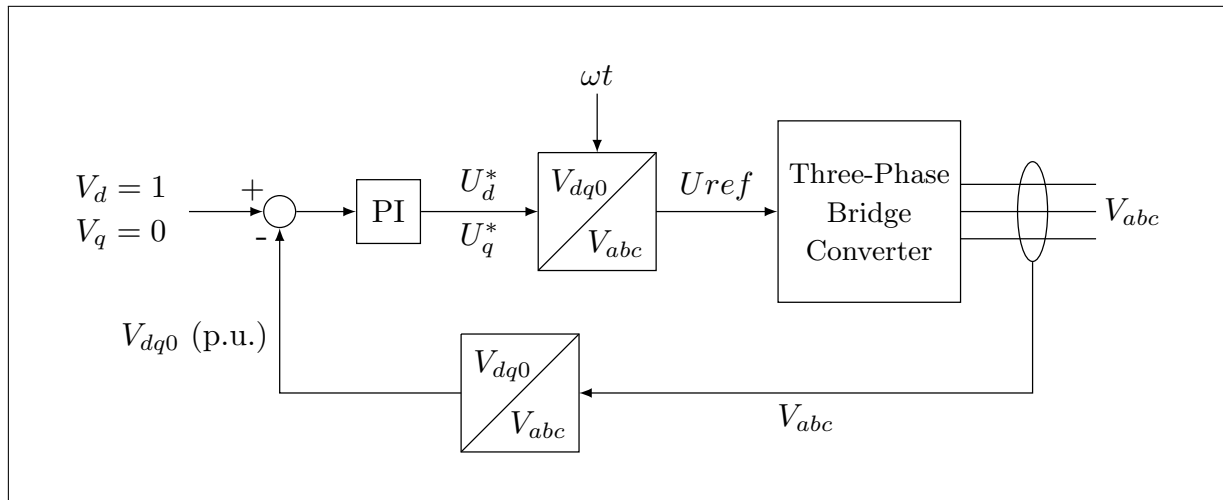


Figure 6.6: Control system structure for a grid forming inverter.

To maintain the grid voltage, the controller measures the AC output voltage, shown on the right. Measured voltage is park transformed into the dq0 reference frame. The feedback is compared with

reference, setting $V_d = 1$ and $V_q = 0$. The error is fed to a PI regulator that generates the control output U_d^* and U_q^* .

Figure 6.7 shows the measured outputs from a three-phase grid forming inverter. The AC frequency reference is set at 60 Hz. AC output voltage reference (Line-Line VRMS) is set at 260V.

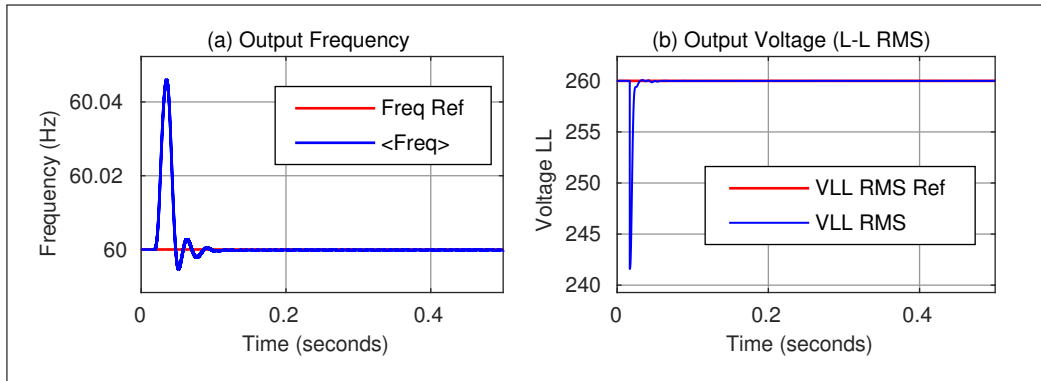


Figure 6.7: Grid forming inverter output measurements.

6.5 Three-phase bridge converter as a Grid Following / Grid Supporting Inverter

A grid forming inverter, as described in previous section, acts as the frequency master in an AC grid. Grid topologies, like the one described in section 2.2, have inertial power sources connected in parallel to the AC grid. In such topologies, it is more economical to setup a generator as the grid frequency master. Synchronization of inertial power sources such as generators require synchronization controller. Such controllers increase the upfront cost and add complexity to the system. Therefore, an inertial power source is setup as the frequency master and other sources act as grid frequency follower that are in phase with the master. An inverter setup in this configuration is known as a grid following or grid supporting inverter [42]. The grid frequency master can be a stiff AC grid such as the utility grid, or it might be an AC synchronous generator or another inverter that acts as a grid forming inverter.

6.5.1 Inverter Control

The controller is implemented in the rotating dq0 reference frame of the grid voltage. An AC power source can be visualized as a resistive element that injects real power into the AC grid. For a power source the d axis is a positive value. To ensure that the injected power is real, the controller ensures that the q axis is force to zero, ensuring the power factor is unity. Figure 6.8 shows the controller for a grid supporting inverter. The power flow is from the DC (left side) to the AC grid (right side). The control algorithm is similar to the rectifier control. The difference is in the flow of power. In a rectifier, the power flow is from AC to DC and reverse in an inverter.

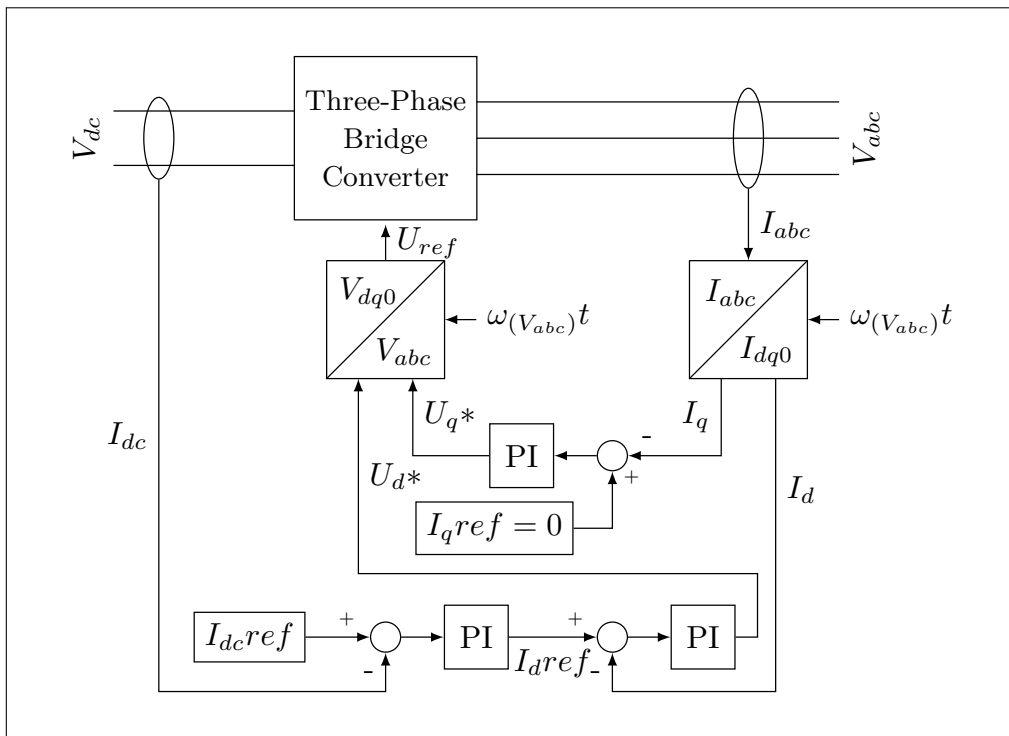


Figure 6.8: Control system structure for a grid Supporting inverter

Intended application of the inverter is in microgrids where the primary objective is to sustain grid stability in events of load change. This requires that an inverter would inject required amount of power into the grid when required. The AC grid frequency and voltage is maintained by the frequency master. Thus, to achieve the stated objective of controlling the amount of injected power into the grid, the inverter controller is setup as a controlled current source.

The control of a grid supporting inverter is similar to a PWM rectifier. It is based on the unity power factor condition. The controller measures the DC input current I_{dc} . The measured current is compared to a reference current value. The reference current determines the amount of power pulled from the DC side, or the amount of power being injected into the AC grid. The error is fed to a PI regulator that outputs a control signal I_{dref} .

The AC side of the controller is implemented in the dq0 reference frame. Controller measures the AC output current shown as i_{abc} . The current is in the abc stationary reference frame. The measured AC grid current is Park transformed fixed in the reference frame of the voltage rotating at (V_{abc}) . The inverter is setup as a real power source. To achieve the unity power factor condition, measured current for the q axis, I_q is compared to a reference value $I_q = 0$. Error from the comparison of reference and measured q axis is fed to a PI regulator that outputs the control value U_q^* .

For the control of d axis, the I_{dref} , from the dc current controller is compared with the measured I_d value. Error value is fed to a PI regulator that generates the control output U_d^* . Control outputs U_d^* and U_q^* are inverse Park Transformed to the abc reference frame to generate U_{ref} . A space vector modulator then drives the semiconductor switches in the bridge converter. Simulink implementation of the grid supporting inverter/rectifier with controller is shown in Figure 6.9. In the figure the controller is integrated with the power electronic components. The controller acts as an inverter/rectifier depending upon the value of reference d-axis current. Notice the 'sel' input port. The port selects the rectifier operation as a constant current or constant voltage output mode. All the measurements are channeled through a measurement bus output port. Fast decaying dynamics are introduced in the upper right corner. These are inserted to break algebraic loops.

Algebraic loops are algebraic constraints that arise in systems that are described by differential algebraic equations or DAE. DAE are equations that describe a system containing additional constraints that have an independent variable and the state variable but does not contain derivative of the state variable. This constraint adds additional computation overhead as the solver must solve the constraint before solving the ODE. In Simulink, algebraic loops occur when a signal loop exists

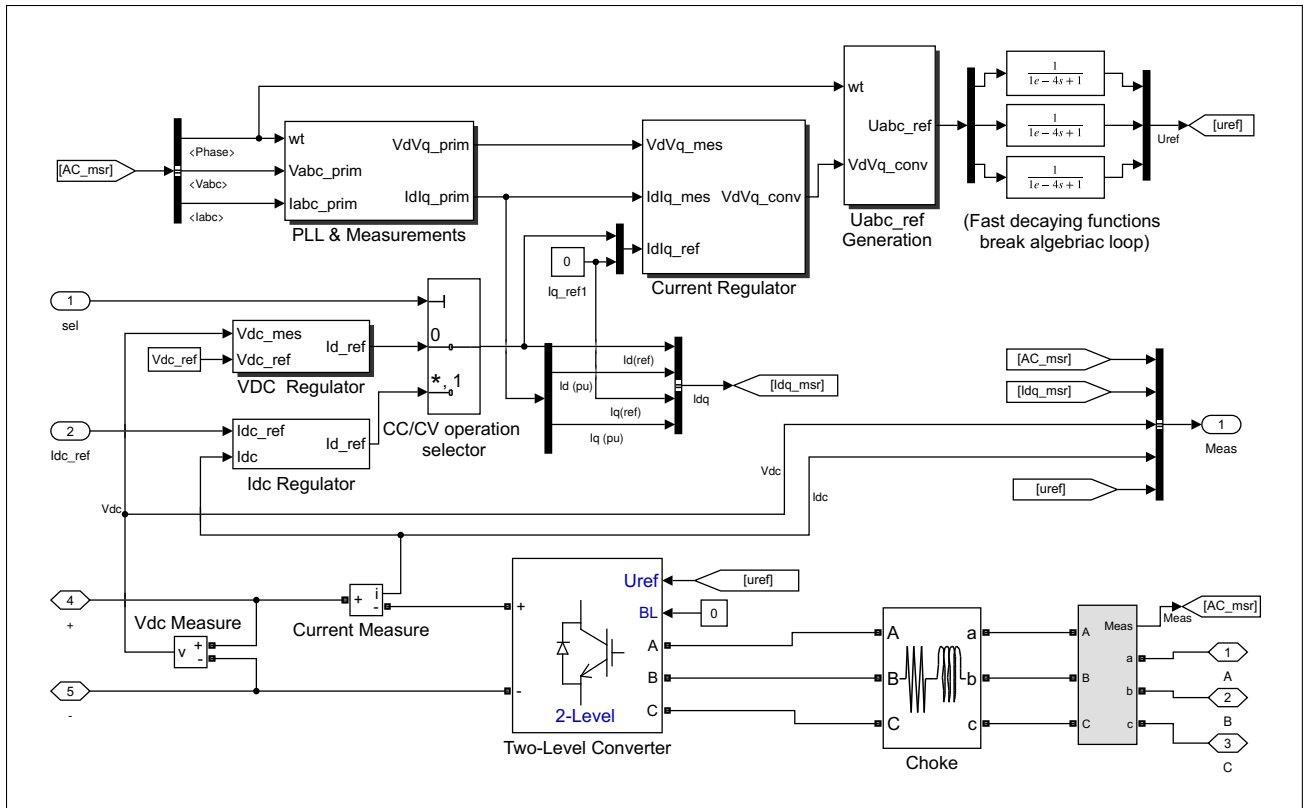


Figure 6.9: Grid supporting inverter Simulink implementation

with only direct feedthrough blocks within a loop. The system cannot be solved if the input port value is not known. Algebraic loops can be avoided by breaking direct feedthrough paths [43]. This is achieved by inserting a delay in the path, such as a fast decaying dynamic shown in Figure 6.9. Algebraic loops might slow down a simulation due to the additional computations. Also, a model containing algebraic loops cannot be compiled into an executable.

Figure 6.10 shows the controller GUI and the parameters mask. The same controller can be used as an active bridge rectifier. The controller mask displayed here only contains the control system. The associated power electronic components are implemented separately.

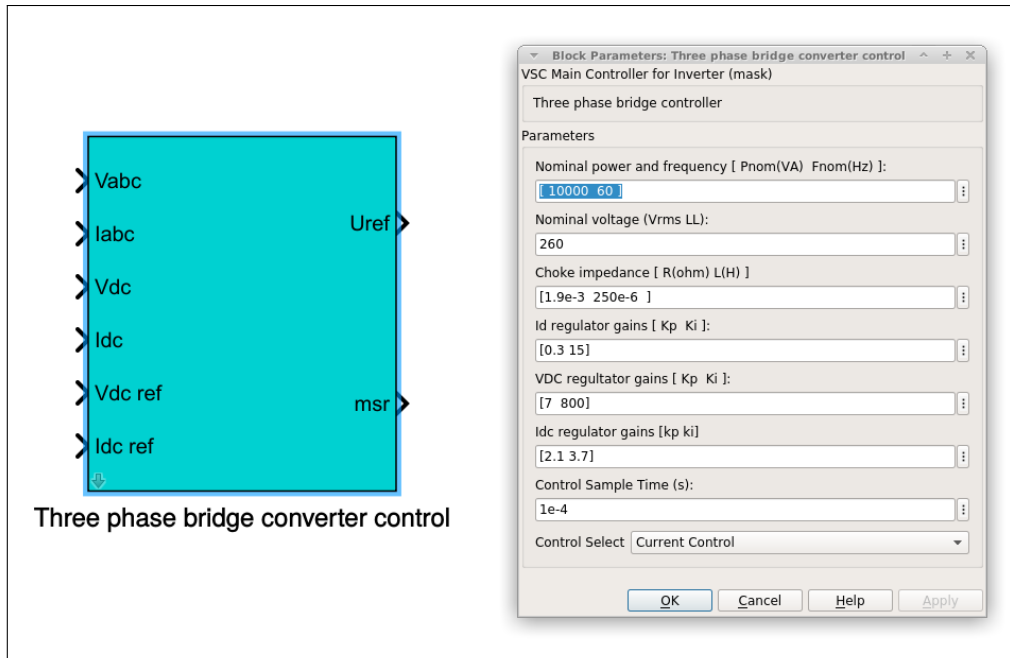


Figure 6.10: Grid following inverter controller GUI and the parameters mask

Figure 6.11 shows output waveforms from a grid supporting inverter. Figure 6.11(A) shows the reference input DC current and the measured value. Figure 6.11(c) shows the reference and the measured I_d . Notice that the reference I_{dref} is positive, thus, bridge converter acts as a DC to AC power converter.

The library and its constituent tools are summarized in Appendix D.

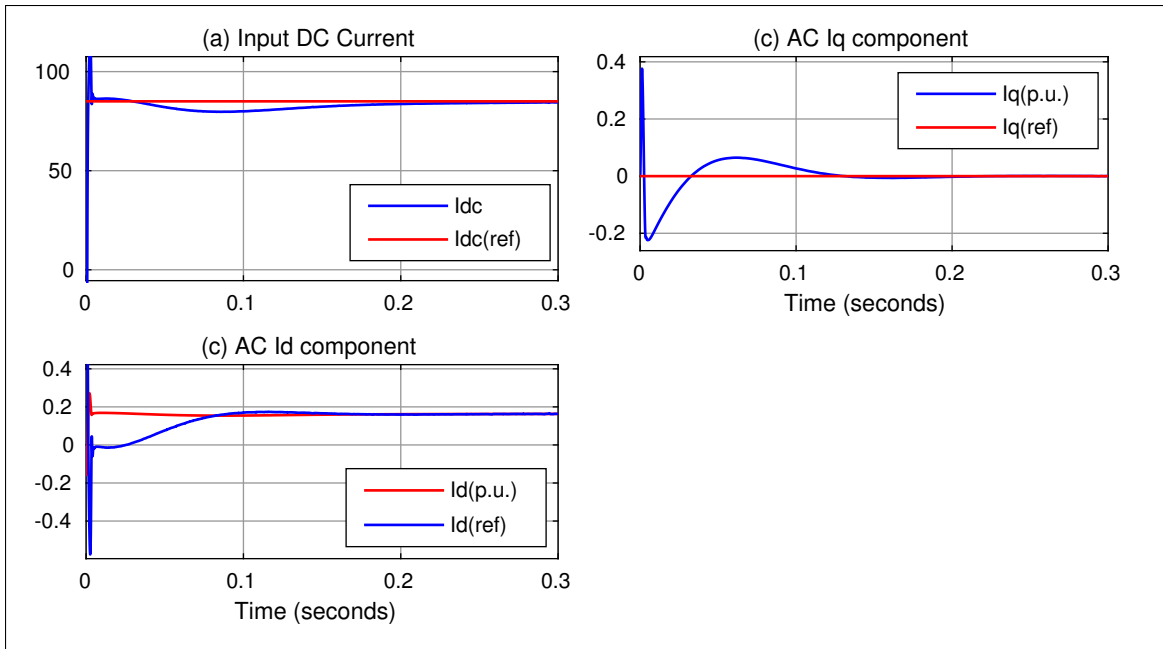


Figure 6.11: Measurements from a grid supporting inverter

Chapter 7

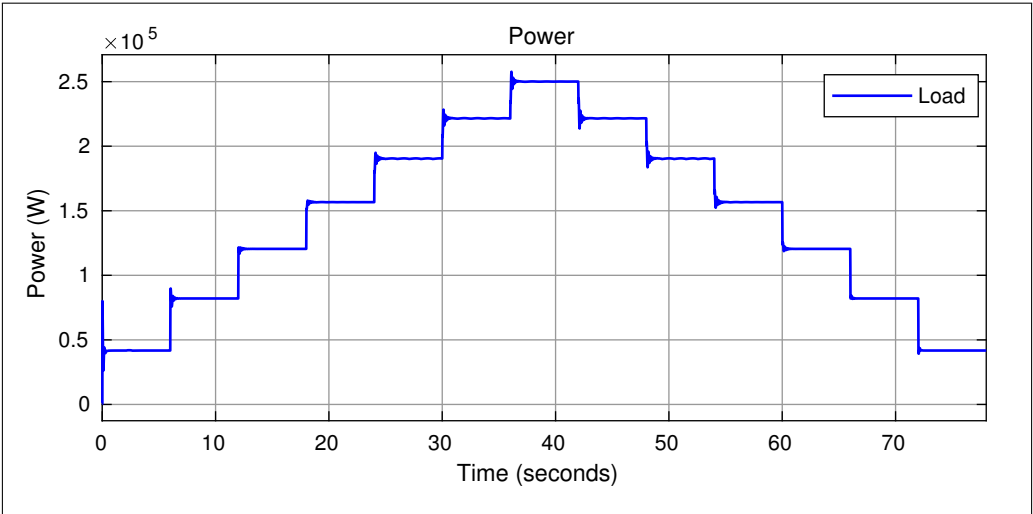
Microgrid Simulation

Internal combustion engines find widespread use in microgrids as the engines provide source of power. Section 3.1.1 describes the transient response of a natural gas engine to load changes. It is observed that natural gas engine exhibits significant deviations in the engine speed when subjected to step load. This makes natural gas engines unsuitable for use in small scale microgrid installations as they would induce unacceptable fluctuations in the grid frequency. Thus they only find limited usage in large power plants that operate in baseload operation, such as in utility grid. As a baseload generator, the engine is not subject to large load fluctuations. Moreover, any large load fluctuation is absorbed by the high inertia of the generator. In small grid installations, such as a microgrid, any load variation directly affects the grid frequency. This issue can be mitigated by combining the natural gas engine with other micro-sources and by employing suitable control schemes.

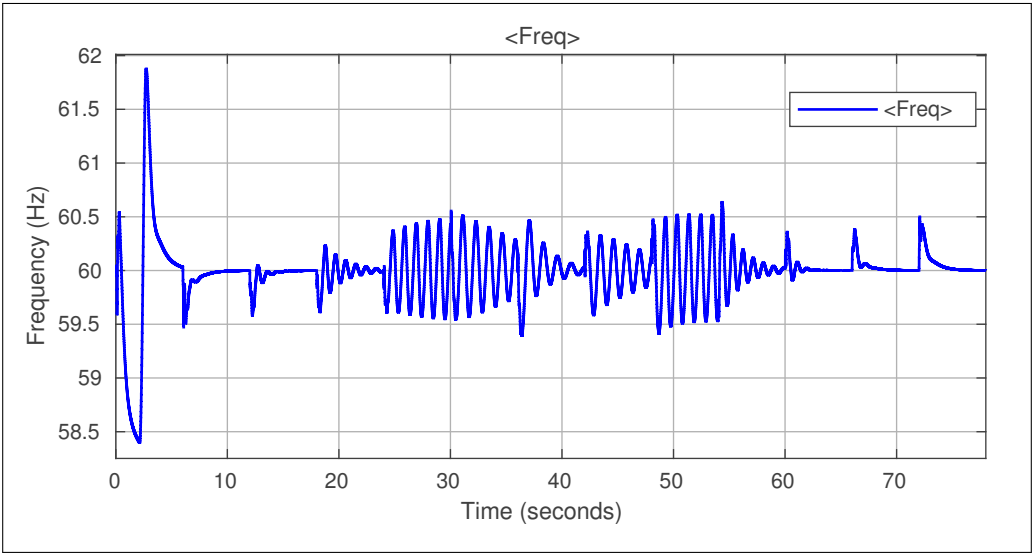
One such microgrid control scheme developed by Han and associates uses a battery energy storage system coupled with a natural gas engine [1] [44]. The battery storage system acts as an energy pool, that is used to inject power into the system in the event of a load change thus reducing the load on the engine. A multi input multi output (MIMO) controller controls the engine and battery. The MIMO controller also controls the battery state of charge (SOC).

This chapter describes the simulation of a microgrid built using the tools described in previous chapters. To set a benchmark for comparison, a natural gas engine generator is run in standalone mode. The engine drives a synchronous generator that powers a load. The engine speed is controlled using a PID regulator. This PID regulator is carefully tuned to extract the best transient response. The load consists of resistive elements connected in series. Each load element is connected with a breaker. The breakers operate at fixed times, generating a staircase load profile. Total simulation run time is 78 seconds. Load step size is 42 kW. Figure 7.1 shows the load profile and the microgrid frequency. Notice that, for a step change in the load, the engine exhibit fluctuations

in the output frequency leading to significant deviation from the grid reference frequency. Change in the engine RPM is the result of changing torque on the engine.



(a) Generator load profile.



(b) Standalone natural gas engine powered generator frequency output.

Figure 7.1: Natural Gas Engine powered generator output.

Next section describes a microgrid configuration that addresses this problem. It will describe the microgrid setup, microgrid control system and the use of the library components developed in the previous chapters to develop a full fledged microgrid simulation.

7.1 Natural Gas Engine Based Microgrid with attached Storage System

Control requirements for the microgrid are as follows. Grid frequency must be maintained at the set reference value. This is achieved by controlling the engine speed. The attached storage system acts as an energy pool that injects power into the grid when there is a deviation in the grid frequency. Battery system should be responsive, while at the same time, giving up control when the grid frequency stabilizes. In a steady state situation, when the grid frequency shows zero deviation, the battery should be charged to maintain the reference state of charge.

Figure 7.2 shows the microgrid setup with an attached storage system. Primary microsource is a synchronous generator powered by a natural gas engine. All the power sources and sinks connect to an AC bus. The battery storage system consists of a bidirectional three-phase bridge converter, shown as an AC-DC block.

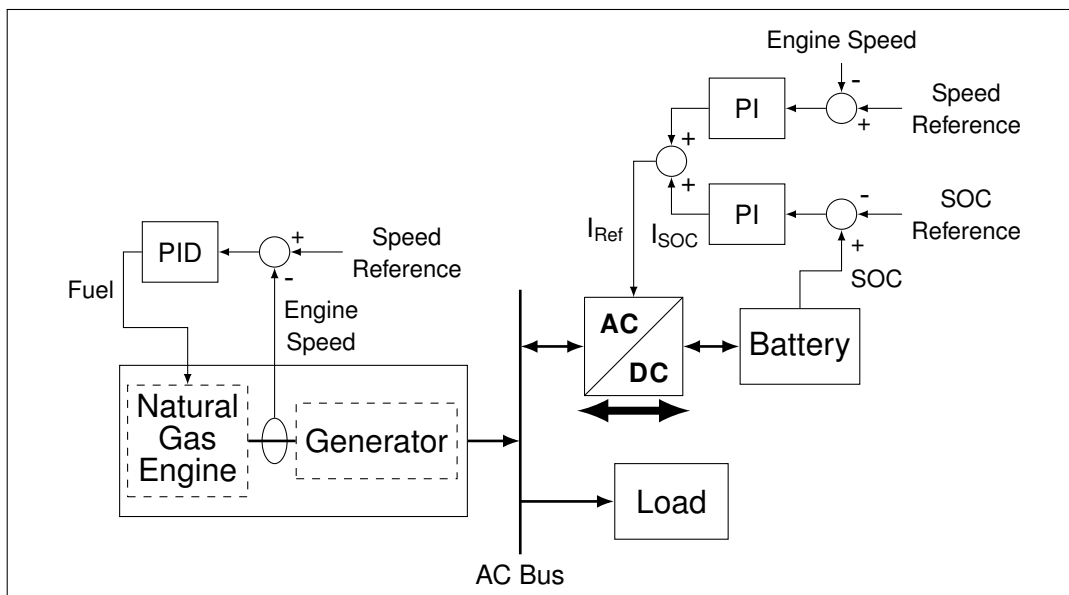


Figure 7.2: Microgrid control with attached storage system.

The converter is setup as a bidirectional inverter-rectifier. The natural gas engine generator is the primary microsource and acts as the grid frequency master. Grid frequency is controlled by the

speed governor in the engine. The converter acts as a grid supporting inverter when power flow is from the battery to the AC grid. It acts as a controlled rectifier when power flows from the AC grid to the battery (charging). Sections 6.3 and 6.5 describe the operation and control system for a rectifier and a grid supporting inverter.

The engine speed is controlled using a PID regulator. Speed reference is set at 1800 rpm. Engine AFR, that determines the engine efficiency, is controlled using a separate PID controller (not shown). Engine drives a synchronous generator connected to the AC bus. The load consists of a series of resistive elements. The load profile is the similar to the one shown in Figure 7.1a.

The engine and the battery storage system work in tandem to stabilize the grid frequency. Battery storage control system is implemented using classical PI regulator. The battery controller consists of a PI regulator that commands a control output in the form of current. The SOC controller controls the state of charge of the battery.

A change in the load leads to change in the torque experienced by the engine. This causes deviation in the engine speed and eventually the grid frequency. Error output from the measured engine speed and the reference engine speed is fed to the PI regulator in the battery controller. The PI regulator outputs a control command shown the figure as I_{ref} .

The bridge converter is setup as a grid supporting inverter when it acts as a power source. The battery controller output I_{ref} is the reference d-axis current for the inverter controller. A load increase in the grid would cause a drop in the engine speed. The resulting error is fed to the battery controller. The battery controller gains are tuned so that the battery controller is responsive but at the same time the controller should account for zero steady state output. Therefore the integral gain is kept small. The proportional gain is set to a high value thus making the system responsive. The microgrid with the attached battery storage system is built using the tools described in previous chapters. System specifications are described below:

Table 7.1: Microgrid system specifications

| Subsystem | Specifications | Details |
|------------------|-------------------------|--|
| Engine | Type | Pre-mixed lean burn natural gas engine |
| | Dispalcement | 20 Liters |
| | Engine Speed | 1800 rpm |
| Generator | Type | Three-phase synchronous salient pole |
| | Pole Pairs | 4 |
| | Voltage (line-line rms) | 260 V |
| | Frequency | 60 Hz |
| | Rated Power | 300 kW |
| Battery | Type | Lithium-ion |
| | Nominal Voltage | 450 V |
| | Capacity | 50 Ah |

Figure 7.3 shows Simulink implementation of the microgrid. The blocks depicted in the figure are sourced from the library components described in previous chapters. The natural gas engine model block was described in Chapter 3. The inverter-rectifier block was described in Chapter 6.

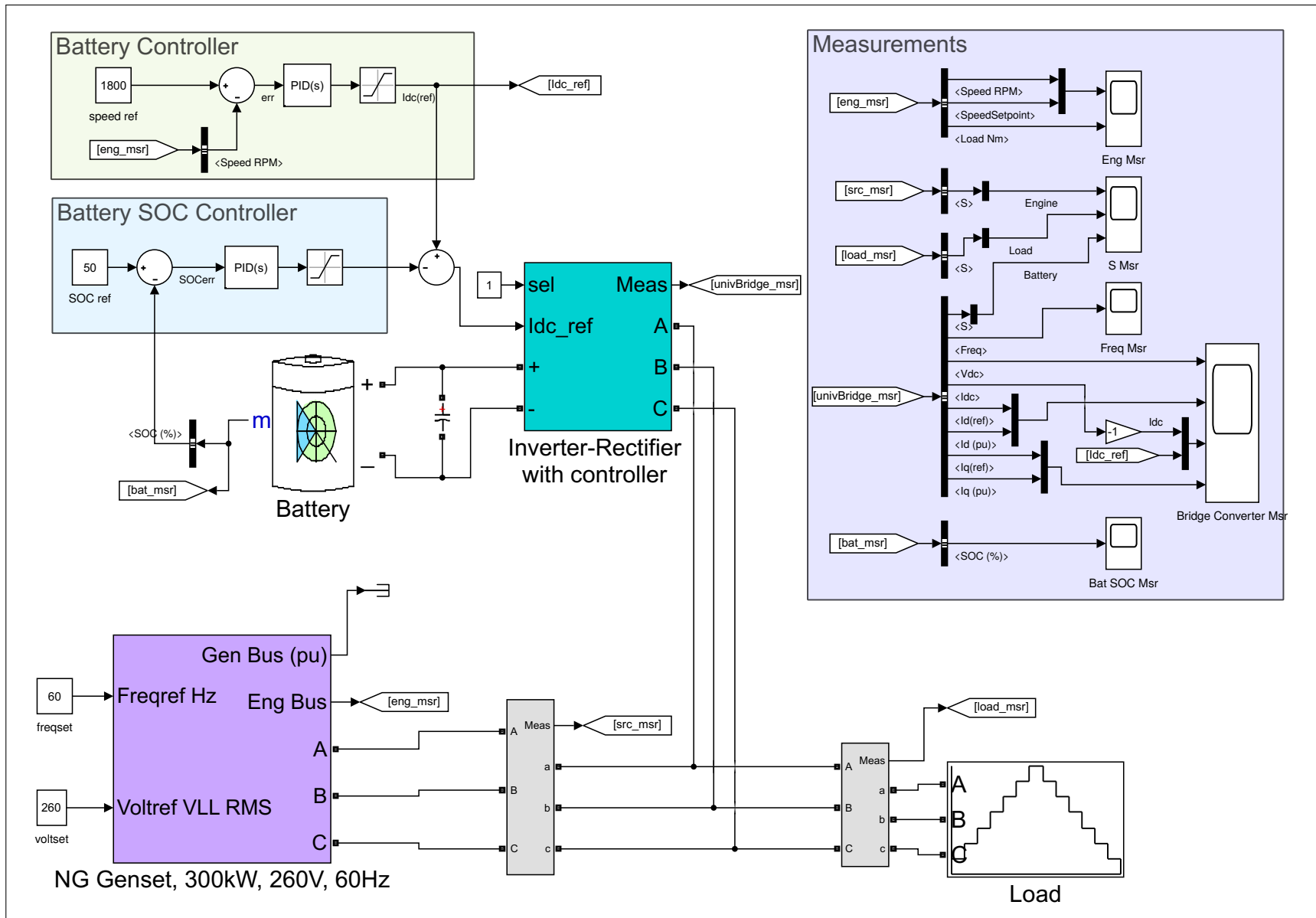


Figure 7.3: Simulink implementation of the microgrid

Simulation run time was 78 seconds. Figure 7.4 shows the grid frequency. Comparing it with the grid frequency of the microgrid consisting of a standalone natural gas engine genset shown in Figure 7.1b, the frequency deviation is considerably reduced. A standalone generator, shows frequency deviations of more than 0.6 Hz, with an initial frequency deviation exceeding 1.5 Hz. The proposed microgrid setup shows frequency deviations of less than 0.4 Hz. Standalone system also exhibits sustained oscillations after the fourth step. In the battery storage supported microgrid, the deviation is significantly reduced and at the same time resulting in zero oscillations. For each step change in the load, the frequency stabilizes in about 5 seconds. One can thus conclude that the proposed microgrid and the control system are effective.

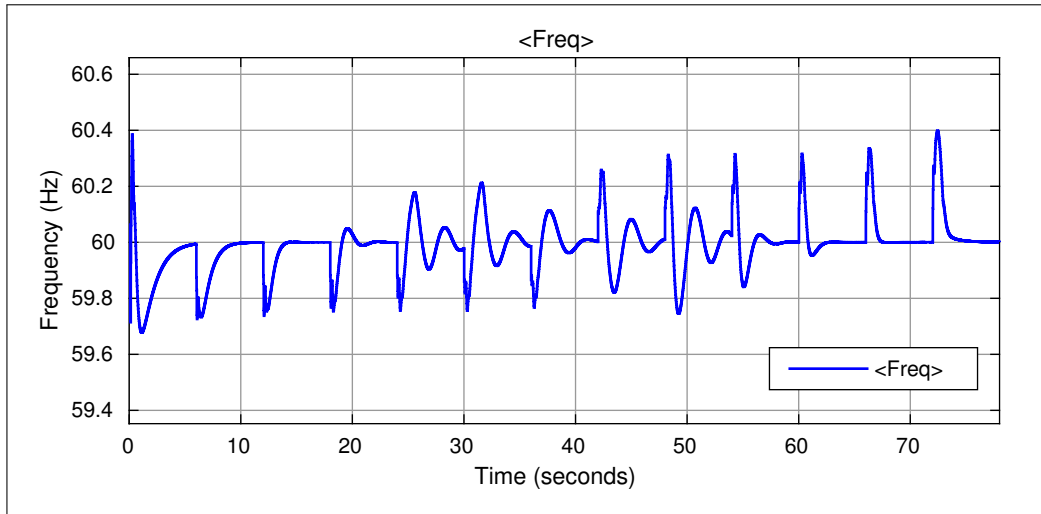


Figure 7.4: Microgrid control with attached storage system.

Figure 7.5 shows the apparent power share for the three systems. The solid line is the power consumed by the load. Engine power output is the plot superimposed on the load. In case of frequency deviation, the PI controller promptly responds to inject power into the grid. This shows up as a spike in the battery power output at the bottom of the graph. Power share of the system during a positive error in the engine speed is described in equation 7.1.

$$P_{Load} = P_{Gen} + P_{Bat} \quad (7.1)$$

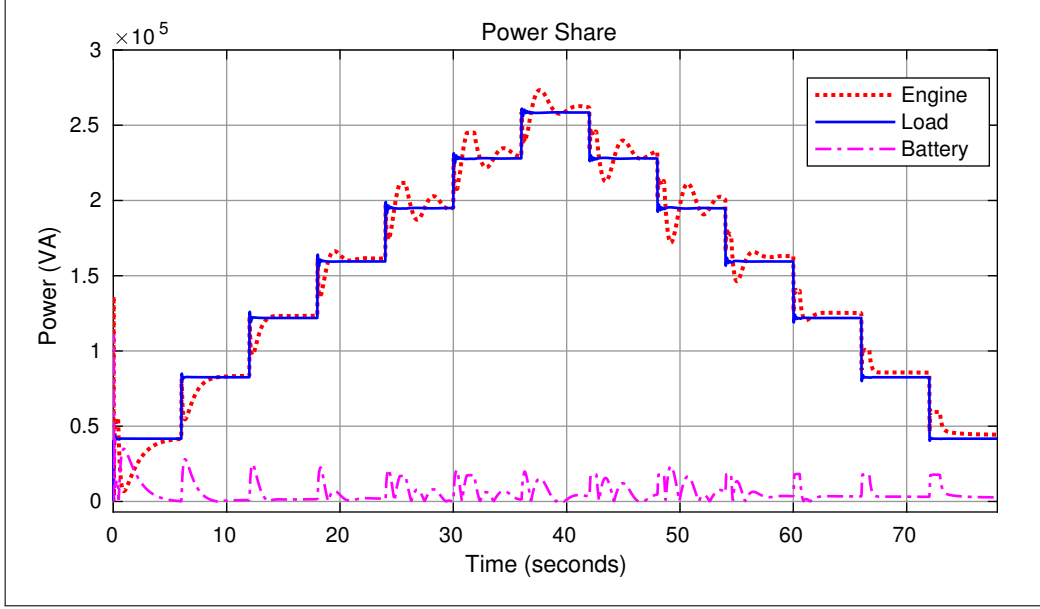


Figure 7.5: Microgrid power share.

Total power consumed by the load P_{Load} is the sum of power output of the generator and the power injected into the grid by the inverter. Notice that, after the grid frequency reaches steady state, engine output resumes normally and the inverter output reduces.

As stated in the requirements, the microgrid controller must charge the battery when the system is running in steady state. This is achieved by the battery state of charge controller. The controller compares the reference SOC value with the measured battery SOC and feeds the error to a PI regulator generating the control output SOC. Bridge converter control variable I_{ref} determines the power flow in the bridge converter. In steady state, the grid maintains the grid frequency, deactivating the battery controller. This leads to a negative I_{ref} , causing the bridge converter to act as a rectifier, pulling power out from the grid into the battery. The rectifier is setup as constant current source. Power share for the system when the bridge converter is acting as a rectifier is given as

$$P_{Gen} = P_{Load} + P_{Bat} \quad (7.2)$$

Power output from the generator is shared between the load and the rectifier. The additional power drawn by the rectifier shows up as an offset in the generator power output shown in Figure 7.5. The battery state of charge is shown in Figure 7.6.

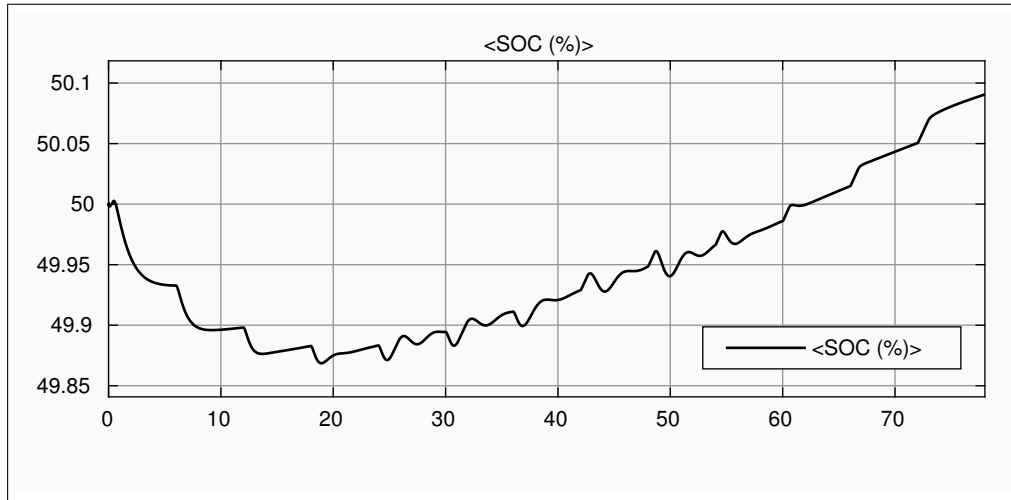


Figure 7.6: Battery State of Charge.

Notice that there is a steep drop in the SOC value in the beginning. This corresponds to the large frequency deviation observed in the beginning. As the simulation progresses, the time for which the battery is discharging is smaller than the time it is charging. This shows up as an eventually increasing SOC. Control output from the SOC controller is clamped so that the engine is not loaded when charging the battery. Failure to do so would lead to increased load on the engine, eventually causing a drop in the engine rpm. This would cause undesirable oscillations in the system.

7.2 Optimized settings for simulation

This section lists out some recommended solver settings and techniques that might be helpful for setting up an efficient Simulink simulation based on our experience to date with these simulation systems.. These simulations are specific to the Simulink software. Some techniques and options are dependent on license type. Refer to the MATLAB or Simulink website for details.

7.2.1 Power Electronics Devices modeling

The power electronics components are modeled using different techniques. User can select the appropriate model from the system mask. The different modeling techniques are described below.

Switching Devices Model

The device is modeled using detailed semiconductor device models. Such a model simulates transients and individual semiconductor device characteristics. Using this model, A designer can simulate and analyze the system for total harmonic distortion (THD) etc. The switching devices model provides the most accurate simulation results but leads to slower simulation.

Switching Function Model

The power electronics device is modelled using voltage and current sources to mimic the switching. It does not simulate the underlying physics of the semiconductor devices. The model generates harmonics and thus, can be used to analyze the same. Simulations built using this type of model run faster than switching devices mode.

Average Characteristics Model

In an average model, the semiconductor devices are replaced by averaged current and voltage sources. For example, an ideal a single quadrant buck or boost converter (with zero losses) can be described by the conservation of energy relation. Thus, input and output power must be equal. The average model is not driven by pulses and thus, does not simulate switching or harmonics. This model provides the fastest simulations.

The work presented in this text is directed towards research in microgrid control. The simulations would simulate transient response of the various subsystems and their behavior during load variations and source transitions etc. All the simulations developed in the previous chapters were based on average characteristic models. A typical simulation run using the average characteristics model is about four times faster than simulation using switching devices models.

7.2.2 Miscellaneous settings

The simulation execution time can be drastically cut by running it in rapid accelerator mode. In rapid accelerator mode, the models are converted into equivalent C or C++ code. The generated code is then compiled and run. A typical simulation setup in rapid accelerator mode runs about three to four times faster than in normal mode. Ability to run a simulation in rapid accelerator mode is subject to toolbox dependencies and license type.

The engine models described in Chapter 3 execute in least time when solver is set to "ode23tb" (trapezoidal rule + backward differentiation formula) solver. Simulations can be made to run faster by disabling the zero crossing detection [45]. However, this may cause a deterioration in the accuracy of the simulation. User must exercise caution and weigh the trade-offs.

Chapter 8

Conclusion and Future Work

The thesis implements a microgrid simulation based on a natural gas engine. Governments and environmental agencies have been tightening the emission norms for quite a few years. This is due to an increasing number of vehicles and overall fuel consumption on the planet. Stringent emission standards are necessitated due to increasing pollution in the cities. Diesel engines have been specifically targeted due to high particulate matter in the diesel engine exhaust emissions. Diesel engines have a fast transient response to big load changes as shown in Chapter 3. This is the reason they find widespread use as backup generators. Increasingly stringent emission standards have put pressure on the manufacturers to improve engine efficiency and at the same time cutting down on the emission. The very nature of a diesel fuel engine makes this difficult. High engine temperature combined with lower refined fuel makes it harder to meet the emission standards. This has led to companies resorting to unethical practices, to cut cost. A good example would be the Volkswagen scandal that involved cheating emission tests by tampering with the diesel engine during inspections [46]. This incident was an eyeopener for the industry. This led to stricter monitoring and vigilance. Keeping these factors in mind, manufacturers either have to invest more in reducing exhaust emissions or switch to alternate and cleaner sources of fuel such as natural gas. The proposed microgrid and the simulation described in this thesis provides an alternative to diesel engine based microgrid.

Public awareness about climate change and adverse effects due to overuse of fossil fuels has shifted the public opinion. Today's customer is more informed and educated. This changes the cost dynamics and economics of the energy industry. Today corporations, besides selling services, sell value based services. In this type of model, consumers pay more for an otherwise cheaper service in return for that added value which would otherwise have been cheaper. This model is applicable to energy industry too. Consumers are willing to pay more for energy from a clean energy source rather than cheaper conventional sources such as coal etc. This push towards cleaner

energy sources is good news for the microgrid technologies as microgrids incorporating renewable energy sources would see a more widespread implementation, creating new jobs.

The work done in this thesis lays down a groundwork for future research in the area of microgrids. The systems described in this thesis are compiled into a Simulink library. The thesis covered various topics related to microgrid systems and their control. Colorado State University has a robust research community and environment that is focused on research into energy technologies. Powerhouse Energy Research Institute is a hub for researchers and companies working on a spectrum of energy technology areas. I hope that the work presented in this thesis would be helpful to future researchers.

8.1 Future Work

8.1.1 Hardware-In-the-Loop Testing

This section lays down potential expansion of modeling and experimentation of proposed techniques and ideas. One such experimentation and validation technique is Hardware in Loop Testing (HIL).

Experimentation and validation of proposed theorems and technologies is an essential part of research. Software simulations is the first step in that direction. The next step in the development of practical deliverable systems is the implementation of actual real-time systems. The efficacy of the control systems developed in simulation environments is limited to those simulations. Practical control systems, implemented in real world applications, are complex systems. The complexity arises from the perspective of controller implementation, communication, data collection and sensing.

The traditional workflow of system design and validation is:

1. Construct mathematical models for the systems to be controlled.
2. Design control methodology for the system.
3. Simulate, test and refine the control system in the simulation environment.

4. Implement the control system on a actual hardware (Industrial controller or microcontroller etc.)
5. Test, validate and refine the real-time control system on a physical test system such that it meets the system performance requirements.

Of all the above-mentioned steps, step 4 and step 5 involves implementation on real-world hardware. The rest of the steps are implemented in software, thus the investment trade-off when compared with hardware based iterative development is high. The cost of setting up a test system requires high level of investment. The process of validation and testing requires significant manpower and time. These issues can be addressed by software systems that replicate the behavior of real-world hardware [47]. This type of a system simulations implementation is called hardware-in-the-loop (HIL) testing.

There are several vendors that supply HIL testing systems that directly integrate with the MATLAB Simulink environment. A few of these are:

- OPAL-RT [48]
- Speed Goat [49]

HIL based system testing gives researchers and designers a lot of flexibility in testing new techniques and methodologies. Future research into microgrids, that would utilize the simulation tools described in this text, would be integrated with an HIL testbed. Thus, researchers would be able to test and implement any new control strategies and techniques on real-time hardware platforms, without having to build physical systems.

8.1.2 Use of alternate storage technologies

Alternate energy storage technologies can be used as a replacement to the battery. Supercapacitor or ultracapacitor is a promising contender. Battery is an energy source that is used to store electric energy over extended periods of time. Analysis of the transient response of the system

described in section 7.1, suggests that the battery is being actively utilized only for small time durations, resulting in minimal battery state of charge variation. As evident in Figure 7.4, the grid frequency stabilizes in a few seconds, suggesting that an energy storage system can be replaced by a power source.

A supercapacitor is a power source that is employed in applications that require low energy density but high power density. Supercapacitors offer some unique advantages over battery storage system. Supercapacitors do not rely on chemical energy for electricity storage, thus have much longer lifespan (charge-discharge cycles). Batteries are accompanied by battery controllers that monitor the charging and discharging. Supercapacitors require less sophisticated management systems [50].

Further research is needed to establish the feasibility and economic viability of using a supercapacitor for use in microgrid for the purpose of frequency stabilization.

8.1.3 Robust MIMO Control of the microgrid

The library components described in this thesis rely on classical single input single output (SISO) PID controllers. Robust control theory is a powerful tool that has numerous advantages over classical PID control and other classical control design techniques. A controller designed for a specific system is only as good as the mathematical model that is used to represent it. Classical control design techniques such as design in frequency domain and time domain typically rely on the assumption that the systems being analyzed are linear and time invariant. This limits the applicability of these design techniques. Actual physical applicability of the classical techniques is limited further as even the systems that are largely linear time invariant, exhibit varying degrees of nonlinearity in practice. Another factor that adds to uncertainty when working on mathematical models representing physical systems is that, the mathematical models cannot precisely model real life physical systems. This is the result of unmodeled nonlinearities, dynamics, and errors in measurement.

Robust control theory provides a sound framework that takes into account the above mentioned shortcomings. A designer can account for uncertainties in modeling and errors in measurements. Classical control design techniques such as PID can only work on single input single output systems. Multiple Input Multiple Output (MIMO) systems have to utilize multiple SISO PID loops that are designed and operated independently. MIMO controllers designed using state space methodology afford the possibility of coordinated MIMO action, but they require precise mathematical model of the system. Using robust control theory, one can design a MIMO controller that is robust to the above mentioned uncertainties.

The tools described in this thesis could be used to design a microgrid that would incorporate a unified MIMO controller that can control the whole system. MIMO controller has been shown to exhibit significantly improved performance over classical PID controlled system [1] [51] [44]. Han has developed MIMO controllers for natural gas engine based microgrid, like the one described in Chapter 7. The MIMO controllers would be added to the library thus providing a rich set of tools. Robust control theory has some unique features that makes it suitable for a wide variety of control tasks. The author wishes to pursue future research in robust control theory and its potential applications in solving various control problems.

Bibliography

- [1] Y. Han, *Microgrid Optimization, Modeling and Control*. Phd Dissertation, Colorado State University, 2014.
- [2] B. News, “Puerto Rico may be months without power,” Sep 2017.
- [3] L. A. Dessaint, K. Al-Haddad, H. Le-Huy, G. Sybille, and P. Brunelle, “A power system simulation tool based on simulink,” *IEEE Transactions on Industrial Electronics*, vol. 46, pp. 1252–1254, Dec 1999.
- [4] “Save a Model - MATLAB & Simulink.” <https://www.mathworks.com/help/simulink/ug/saving-a-model.html>, Apr 2018. [Online; accessed 18. Apr. 2018].
- [5] “How Simscape Power Systems Software Works - MATLAB & Simulink.” <https://www.mathworks.com/help/physmod/sps/powersys/ug/how-simpowersystems-software-works.html>, Apr 2018. [Online; accessed 18. Apr. 2018].
- [6] D. Feldman, “Photovoltaic (PV) Pricing Trends: Historical, Recent, and Near-Term Projections.” <https://www.nrel.gov/docs/fy13osti/56776.pdf>, Sep 2013. [Online; accessed 18. Apr. 2018].
- [7] M. D. Platze, “U.S. Solar Photovoltaic Manufacturing: Industry Trends, Global Competition, Federal Support - R42509.pdf.” <https://fas.org/sgp/crs/misc/R42509.pdf>, Oct 2016. [Online; accessed 18. Apr. 2018].
- [8] K. Kant, C. Jain, and B. Singh, “A hybrid diesel-wind pv-based energy generation system with brushless generators,” *IEEE Transactions on Industrial Informatics*, vol. 13, pp. 1714–1722, Aug 2017.
- [9] Z. Yi, W. Dong, and A. H. Etemadi, “A unified control and power management scheme for pv-battery-based hybrid microgrids for both grid-connected and islanded modes,” *IEEE Transactions on Smart Grid*, pp. 1–1, 2017.

- [10] Q. C. Zhong and G. Weiss, "Synchronverters: Inverters that mimic synchronous generators," *IEEE Transactions on Industrial Electronics*, vol. 58, pp. 1259–1267, April 2011.
- [11] J. Rocabert, A. Luna, F. Blaabjerg, and P. Rodr guez, "Control of power converters in ac microgrids," *IEEE Transactions on Power Electronics*, vol. 27, pp. 4734–4749, Nov 2012.
- [12] J. Heywood, *Internal Combustion Engine Fundamentals*. Automotive technology series, McGraw-Hill, 1988.
- [13] E. Alfieri, A. Amstutz, and L. Guzzella, "Gain-scheduled model-based feedback control of the air/fuel ratio in diesel engines," *Control Engineering Practice*, vol. 17, no. 12, pp. 1417–1425, 2009.
- [14] "Alternative Fuels Data Center: Fuel Prices." <https://www.afdc.energy.gov/fuels/prices.html>, Apr 2018. [Online; accessed 18. March. 2018].
- [15] P. Krause, O. Wasynczuk, S. D. Sudhoff, and S. Pekarek, *Analysis of electric machinery and drive systems*, vol. 75. John Wiley & Sons, 2013.
- [16] "Ieee recommended practice for excitation system models for power system stability studies," *IEEE Std 421.5-2016 (Revision of IEEE Std 421.5-2005)*, pp. 1–207, Aug 2016.
- [17] R. H. Lasseter, "Microgrids," in *2002 IEEE Power Engineering Society Winter Meeting. Conference Proceedings (Cat. No.02CH37309)*, vol. 1, pp. 305–308 vol.1, 2002.
- [18] A. Tuladhar, H. Jin, T. Unger, and K. Mauch, "Parallel operation of single phase inverter modules with no control interconnections," in *Proceedings of APEC 97 - Applied Power Electronics Conference*, vol. 1, pp. 94–100 vol.1, Feb 1997.
- [19] J. D. Glover, M. S. Sarma, and T. Overbye, *Power System Analysis & Design, SI Version*. Cengage Learning, 2012.

- [20] V. C. Gungor, D. Sahin, T. Kocak, S. Ergut, C. Buccella, C. Cecati, and G. P. Hancke, “A survey on smart grid potential applications and communication requirements,” *IEEE Transactions on Industrial Informatics*, vol. 9, pp. 28–42, Feb 2013.
- [21] K. Tomsovic, D. E. Bakken, V. Venkatasubramanian, and A. Bose, “Designing the next generation of real-time control, communication, and computations for large power systems,” *Proceedings of the IEEE*, vol. 93, pp. 965–979, May 2005.
- [22] A. Mohd, E. Ortjohann, W. Sinsukthavorn, M. Lingemann, N. Hamsic, and D. Morton, “Isochronous load sharing and control for inverter-based distributed generation,” in *2009 International Conference on Clean Electrical Power*, pp. 324–329, June 2009.
- [23] P. Hersch and K. Zweibel, “Basic photovoltaic principles and methods,” tech. rep., Solar Energy Research Inst., Golden, CO (USA), 1982.
- [24] A. Goetzberger and V. U. Hoffmann, *Photovoltaic solar energy generation*, vol. 112. Springer Science & Business Media, 2005.
- [25] “Libraries and Databases | System Advisor Model (SAM).” <https://sam.nrel.gov/libraries>, Apr 2018. [Online; accessed 18. Apr. 2018].
- [26] “Implement PV array modules - Simulink,” Apr 2018. [Online; accessed 18. Apr. 2018].
- [27] T. Esum and P. L. Chapman, “Comparison of photovoltaic array maximum power point tracking techniques,” *IEEE Transactions on Energy Conversion*, vol. 22, pp. 439–449, June 2007.
- [28] F. Liu, S. Duan, F. Liu, B. Liu, and Y. Kang, “A variable step size inc mppt method for pv systems,” *IEEE Transactions on Industrial Electronics*, vol. 55, pp. 2622–2628, July 2008.
- [29] R. W. Erickson and D. Maksimovic, *Fundamentals of power electronics*. Springer Science & Business Media, 2007.

- [30] “Implement boost power converter - Simulink.” <https://www.mathworks.com/help/physmod/sps/powersys/ref/boostconverter.html>, Apr 2018. [Online; accessed 18. Apr. 2018].
- [31] K. Divya and J. Østergaard, “Battery energy storage technology for power systems—An overview,” *Electric Power Systems Research*, vol. 79, no. 4, pp. 511–520, 2009.
- [32] “Implement generic battery model - Simulink.” [?], Apr 2018. [Online; accessed 18. Apr. 2018].
- [33] A. A.-H. Hussein and I. Batarseh, “A review of charging algorithms for nickel and lithium battery chargers,” *IEEE Transactions on Vehicular Technology*, vol. 60, pp. 830–838, March 2011.
- [34] M. Chen and G. A. Rincon-Mora, “Accurate, compact, and power-efficient li-ion battery charger circuit,” *IEEE Transactions on Circuits and Systems II: Express Briefs*, vol. 53, pp. 1180–1184, Nov 2006.
- [35] M. Gholizadeh and F. R. Salmasi, “Estimation of state of charge, unknown nonlinearities, and state of health of a lithium-ion battery based on a comprehensive unobservable model,” *IEEE Transactions on Industrial Electronics*, vol. 61, pp. 1335–1344, March 2014.
- [36] Y. S. Lee, W. Y. Wang, and T. Y. Kuo, “Soft computing for battery state-of-charge (bsoc) estimation in battery string systems,” *IEEE Transactions on Industrial Electronics*, vol. 55, pp. 229–239, Jan 2008.
- [37] R. H. Park, “Two-reaction theory of synchronous machines generalized method of analysis—part i,” *Transactions of the American Institute of Electrical Engineers*, vol. 48, pp. 716–727, July 1929.
- [38] “Perform transformation from three-phase (abc) signal to dq0 rotating reference frame or the inverse - Simulink.” <https://www.mathworks.com/help/physmod/sps/powersys/ref/abctodq0dq0toabc.html>, Apr 2018. [Online; accessed 18. Apr. 2018].

- [39] A. M. Trzynadlowski, *Introduction to modern power electronics*. John Wiley & Sons, 2015.
- [40] “Implement three-phase two-level power converter - Simulink.” <https://www.mathworks.com/help/physmod/sps/powersys/ref/twolevelconverter.html>, Apr 2018. [Online; accessed 18. Apr. 2018].
- [41] N. R. Zargari and G. Joos, “Performance investigation of a current-controlled voltage-regulated pwm rectifier in rotating and stationary frames,” in *Industrial Electronics, Control, and Instrumentation, 1993. Proceedings of the IECON '93., International Conference on*, pp. 1193–1198 vol.2, Nov 1993.
- [42] W. Sinsukthavorn, E. Ortjohann, A. Mohd, N. Hamsic, and D. Morton, “Control strategy for three-/four-wire-inverter-based distributed generation,” *IEEE Transactions on Industrial Electronics*, vol. 59, pp. 3890–3899, Oct 2012.
- [43] “Algebraic Loops - MATLAB & Simulink.” <https://www.mathworks.com/help/simulink/ug/algebraic-loops.html>, Apr 2018. [Online; accessed 18. Apr. 2018].
- [44] Y. Han, P. M. Young, A. Jain, and D. Zimmerle, “Robust control for microgrid frequency deviation reduction with attached storage system,” *IEEE Transactions on Smart Grid*, vol. 6, pp. 557–565, March 2015.
- [45] “Zero-Crossing Detection - MATLAB & Simulink.” <https://www.mathworks.com/help/simulink/ug/zero-crossing-detection.html>, Apr 2018. [Online; accessed 18. Apr. 2018].
- [46] B. News, “Volkswagen: The scandal explained.” <http://www.bbc.com/news/business-34324772>, Dec 2015.
- [47] B. Lu, X. Wu, H. Figueroa, and A. Monti, “A low-cost real-time hardware-in-the-loop testing approach of power electronics controls,” *IEEE Transactions on Industrial Electronics*, vol. 54, pp. 919–931, April 2007.

- [48] “Hardware in the loop xn–bwh HIL simulation xn–bwh OPAL-RT.” <https://www.opal-rt.com/hardware-in-the-loop>, Apr 2018. [Online; accessed 18. Apr. 2018].
- [49] “Hardware-in-the-Loop for Real-Time Plant Simulation - Speedgoat.” <https://www.speedgoat.com/applications-industries/applications/plant-simulation-hil>, Apr 2018. [Online; accessed 18. Apr. 2018].
- [50] S. Werkstetter, “Ultracapacitor usage in wind turbine pitch control systems,” *Maxwell technologies white paper*, p. 5, 2015.
- [51] P. M. Y. Y. Han and D. Zimmerle, “Natural gas engine model for speed and air-fuel control,” *Submitted*, 2015.

Appendix A

MPPT Algorithm

This section describes the pseudo code for the perturb and observe algorithm for maximum power point tracking (MPPT). The routine is computed at every update cycle. The duty cycle step size ΔD is predetermined. D and D_{old} is the output duty-cycle and previous duty-cycle, respectively. V and P is the instantaneous voltage and power. V_{old} and P_{old} is the previous value of the voltage and power. The code section at the end executes saturation limits for the duty cycle.

```
P = V * I
dV = V - Vold
dp = P - Pold
if dP (not equal to) 0
    if dP < 0
        if dV < 0
            D = Dold - deltaD;
        else
            D = Dold + deltaD;
        end
    else
        if dV < 0
            D = Dold + deltaD;
        else
            D = Dold - deltaD;
        end
    end
else
    D = Dold
end

if D >= Dmax (or) D <= Dmin
    D = Dold
end
```

Appendix B

PID Algorithm

The PID controller in a continuous time system is defined as:

$$G_c(s) = K_p + K_i \cdot \frac{1}{s} + K_d \cdot s \quad (\text{B.1})$$

Where K_p is the proportional gain, K_i is the integral gain, and K_d is the derivative gain. This form of a PID controller is called the parallel form. The derivative action in the PID controller responds to instantaneous time rate change of the error. This helps the controller predict any large overshoot ahead of time, thus initiating appropriate control action. A fast changing input or a high frequency noisy input might lead to noisy control signal, thus introducing instability in the system. To remedy this, the derivative term in the controller is modified with a low pass filter. The modified derivative term is defined as:

$$G_D(s) = K_d \cdot \frac{N}{1 + N \cdot 1/s} \quad (\text{B.2})$$

Where, N is the filter coefficient.

Controllers are implemented on digital computers that are discrete time systems. Hence, the equivalent discrete time PID controller is defined as:

$$G_c(s) = K_p + K_i \cdot \frac{T_s}{2} \cdot \frac{z+1}{z-1} + K_d \cdot \frac{N}{1 + N \cdot T_s \cdot (1/(z-1))} \quad (\text{B.3})$$

Where, T_s is the sampling time of the discrete time system.

Appendix C

Additional tools and some implementations

This section lists some additional simulation models. These models source the components and models described in previous chapters.

Generator plus controller with synchronization controller

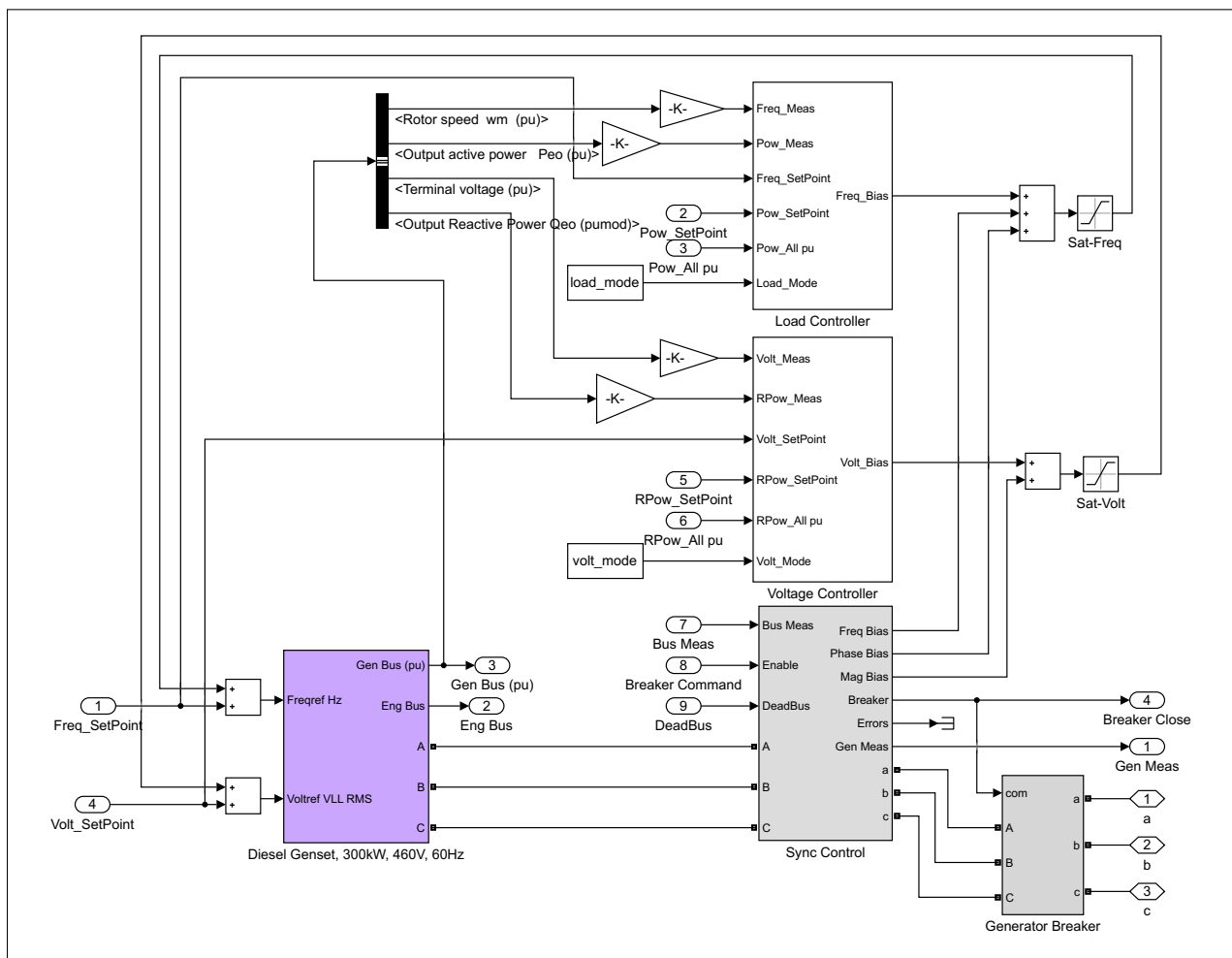


Figure C.1: Generator with controllers for voltage, frequency and synchronization control.

Battery controller example

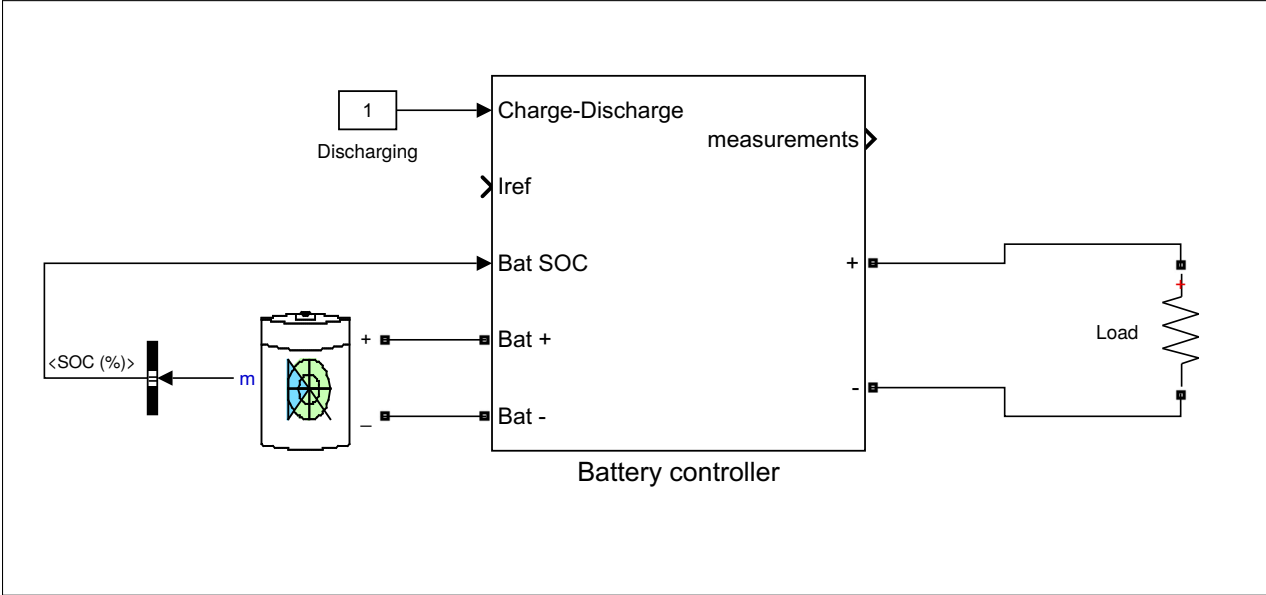


Figure C.2: Battery controller example. Battery controller setup as a constant voltage source powering a load.

Appendix D

Summary of important library components

Here is a summary of the library components:

Base

Contains base components that form the building blocks for any simulation such as measurement blocks, engine models etc.

- Measurement Bus - Line to Neutral
- Measurement Bus - Line to Phase
- Detailed model of a Diesel Engine
- Simple model of a diesel engine
- Detailed model of a natural gas engine
- Simple model of a natural gas engine
- Diesel engine generator
- Natural gas engine generator

Comms

Contains a collection of communication tools. These are used when setting up a multiple generator simulation. These tools are application specific and thus are not listed or described here.

Control

Contains control system models such as engine control, bridge converter control, battery control etc.

- Genset controller - controllers for multiple generator operation

- Genset plus controller - generator and genset controller put in a single model
- Genset plus controller with synchronization controller
- Grid and Power Manager
- Grid Manager
- Three phase bridge converter controller (Grid following inverter)
- Three phase bridge converter controller (Grid forming inverter)
- Battery controller

Renew

Contains tools related to renewable energy such as solar and wind.

- MPPT controller (sourced from Simulink examples)
- Wind turbine model (sourced from Simulink examples)